5

Temperature Measurement of a Surface Exposed to a Plasma Flux Generated Outside the Electrode Gap

Nikolay Kazanskiy and Vsevolod Kolpakov
Image Processing Systems Institute, Russian Academy of Sciences,
S.P. Korolev Samara State Aerospace University (National Research University)
Russia

1. Introduction

Plasma processing in vacuum is widely applied in optical patterning, formation of micro- and nanostructures, deposition of films, etc. on the material surface (Orlikovskiy, 1999a; Soifer, 2002). Surface–plasma interaction raises the temperature of the material, causing the parameters of device features to deviate from desired values. To improve the accuracy of micro- and nanostructure fabrication, it is necessary to control the temperature at the site where a plasma flux is incident on the surface. However, such a control is difficult, since the electric field of the plasma affects measurements. Pyrometric (optical) control methods are inapplicable in the high-temperature range and also suffer from nonmonochromatic self-radiation of gas-discharge plasma excited species.

At the same time, in the plasma-chemical etching setups that have been used until recently, the plasma is generated by a gas discharge in the electrode gap (see, for example (Orlikovskiy, 1999b; Raizer, 1987)). Low-temperature plasma is produced in a gas discharge, such as glow discharge, high-frequency, microwave, and magnetron discharge (Kireyev & Danilin, 1983). The major disadvantages of the above-listed discharges are: etch velocity is decreased with increasing relative surface area (Doh Hyun-Ho et al., 1997; Kovalevsky et al., 2002); the gas discharge parameters and properties show dependence on the substrate's material and surface geometry (Woodworth et al., 1997; Hebner et al., 1999); contamination of the surface under processing with low-active or inactive plasma particles leads to changed etching parameters (Miyata Koji et al., 1996; Komine Kenji et al., 1996; McLane et al., 1997); the charged particle parameters are affected by the gas-discharge unit operation modes; process equipment tends to be too complex and bulky, and reactor designs are poorly compatible with each other in terms of process conditions; these factors hinder integration (Orlikovskiy, 1999b); plasma processes are power-consuming and use expensive gases; hence high cost of finished product.

This creates considerable problems when generating topologies of the integrated circuits and diffractive microreliefs, and optimizing the etch regimes for masking layer windows.

The above problems could be solved by using a plasma stream satisfying the following conditions: (i) The electrodes should be outside the plasma region. (ii) The charged and reactive plasma species should not strike the chamber sidewalls. (iii) The plasma stream

should be uniform in transverse directions. It is also desired to reduce the complexity, dimensions, mass, cost, and power consumption of plasma sources. Furthermore, these should be compatible with any type of vacuum machine in industrial use. Published results suggest that the requirements may be met by high-voltage gas-discharge plasma sources (Kolpakov & V.A. Kolpakov, 1999; V.A. Kolpakov, 2002; Komov et al., 1984; Vagner et al., 1974).

In (Kazanskiy et al., 2004), a reactor (of plasma-chemical etching) was used for the first time; in this reactor, a low-temperature plasma is generated by a high-voltage gas discharge outside the electrode gap (Vagner et al., 1974). Generators of this type of plasma are effectively used in welding (Vagner et al., 1974), soldering of elements in semiconducting devices (Komov et al., 1984), purification of the surface of materials (Kolpakov et al., 1996), and enhancement of adhesion in thin metal films (V.A. Kolpakov, 2006).

This study is devoted to elaborate upon a technique for measuring the temperature of a surface based on the studies into mechanisms of interaction a surface and a plasma flux generated outside the electrode gap.

2. Experimental conditions

Experiments were performed in a reactor shown schematically in Fig. 1a. The high-voltage gas discharge is an anomalous modification of a glow discharge, which emerges when the electrodes are brought closer up to the Aston dark space; the anode must have a through hole in this case. Such a design leads to a considerable bending of electric field lines in this region (Fig. 1b) (Vagner et al., 1974). The electric field distribution exhibits an increase in the length of the rectilinear segment of the field line in the direction of the symmetry axis of the aperture in the anode. Near the edge of the aperture, the length of the rectilinear segment is smaller than the electron mean free path, and a high-voltage discharge is not initiated.

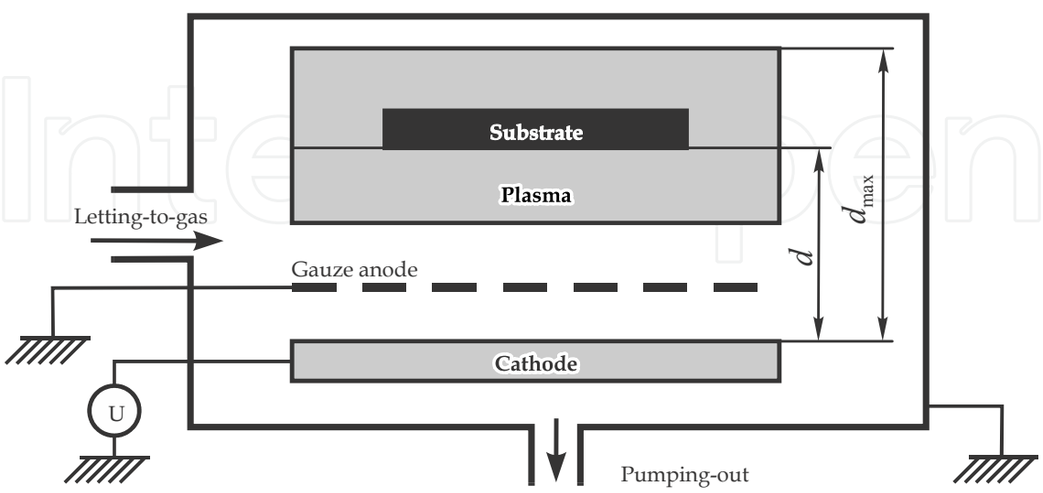

(a)

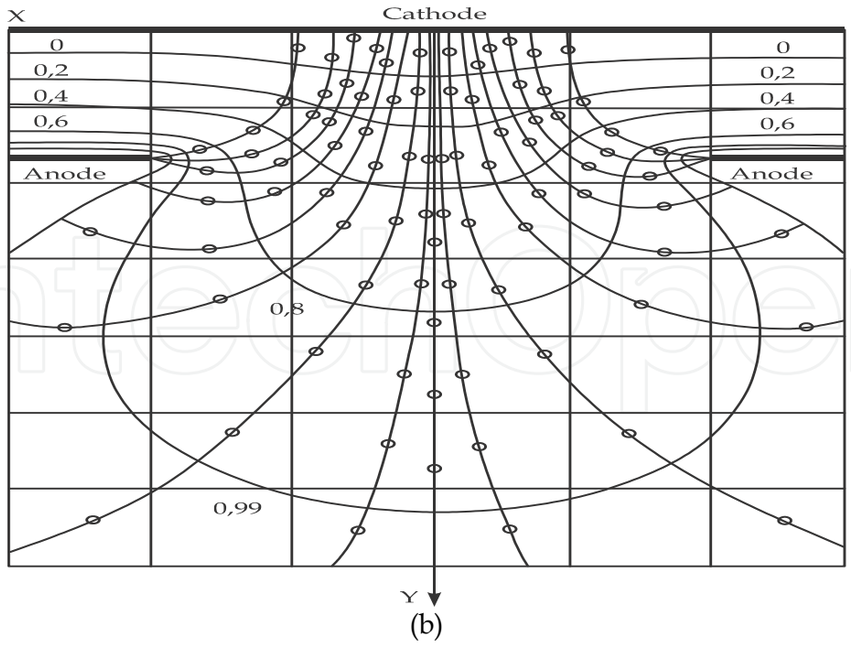

Fig. 1. (a) Schematic of the reactor and (b) field distribution in the near -electrode region of a gas-discharge tube; the mesh size is 0.0018 × 0.0018 m

The electrons emitted from the cathode under the action of the field gradient and moving along the rectilinear segments of field lines acquire an energy sufficient for ionizing the residue gas outside the electrode gap. The majority of positive ions is formed on the rectilinear segments of field lines in the axial zone in the anode aperture and reaches the cathode surface at the points of electron emission. This is confirmed by the geometrical parameters of the spots formed by positive ions on the cathode surface (see Fig. 2). The shape of the spots corresponds to the gauze mesh geometry, while their size is half the mesh size, which allows us to treat this size as the size of the axial region participating in self-sustaining of the charge.

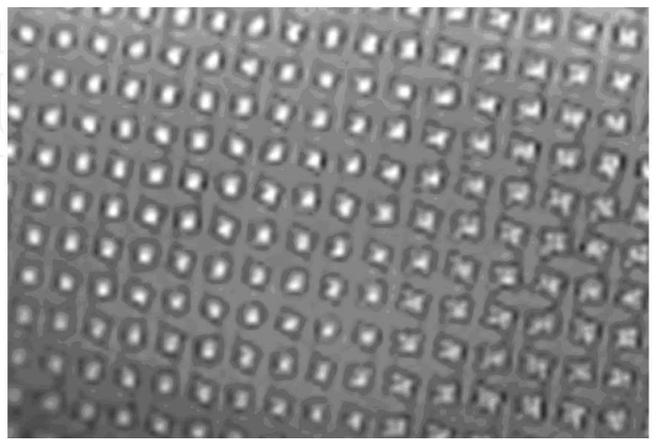

Fig. 2. The shape of spots formed by positive ions on the cathode surface; the spot size is 0.0009 × 0.0009 m

The plasma parameters were measured using collector (Molokovsky & Sushkov, 1991) and rotating probe (Rykalin et al., 1978) methods. To exclude sputtering, the probe was fabricated from a tungsten wire of diameter 0.1 mm, thus practically eliminating any impact on the plasma parameters.

To increase the electron emission, an aluminum cathode was used (Rykalin et al., 1978). To improve the energy distribution uniformity of plasma particles a stainless-steel-wire grid anode of a 1.8 x 1.8 mm cell and 0.5 mm diameter was used, which resulted in a significantly weaker chemical interaction with plasma particles and an increased resistance to thermal heating. This statement can be supported by the analysis of a gas-discharge device described in Ref. (Vagner et al., 1974), with each cell of the anode grid representing a hole and the entire flux of the charged particles being composed of identical micro-fluxes. The microflux parameters are determined by the cell size and the cathode surface properties, which are identical in the case under study and, so are the parameters of the individual microflux. As a result, the charged particle distribution over the flux cross-section will also be uniform, with the nonuniformity resulting only from the edge effect of the anode design, whose area is minimal. For the parameters under study, the uniformity of the charge particle distribution over the flux cross-section was not worse than 98% (Kolpakov & V.A. Kolpakov, 1999). The discharge current and the accelerating voltage were 0-140 mA and 0-6 kV. The process gases are CF_4, CF_4–O_2 mixture, O_2 and air. The sample substrates were made up of silicon dioxide of size 20x20 mm², with/without a photoresist mask in the form of a photolithograpically applied periodic grating, polymer layers of the DNQ based on diazoquinone and FP-383 metacresol novolac deposited on silicon dioxide plates with a diameter of up to 0.2 m (Moreau, 1988a). Before the formation of the polymer layer, the surface of the substrates was chemically cleaned and finished to 10^{-8} kg/m² (10^{-9} g/cm²) in a plasma flow with a discharge current of I = 10 mA, accelerating voltage U = 2 kV, and a cleaning duration of 10 s (Kolpakov et al., 1996). The profile and depth of etched trenches were determined with the Nanoink Nscriptor Dip Pen Nanolithography System, Carl Zeiss Supra 25 Field emission Scanning Electron Microscopes and a “Smena” scanning-probe microscope operated in the atomic-force mode. Cathode deposit was analyzed with a x-ray diffractometer. Surface temperature was measured by a precision chromel–copel thermocouple.

3. Experimental results and discussion of the high-voltage gas discharge characteristics

The high-voltage gas discharge is an abnormal variety of the glow discharge and, therefore, while featuring all benefits of the latter, is devoid of its disadvantages, such as the correlation between the gas discharge parameters and the substrate's location and surface properties.

When the cathode and anode are being brought together to within Aston space, the glow discharge is interrupted because of fulfillment of the inequality $nG<1$, where n and G are the number of electrons and ions, respectively. However, if a through hole is arranged in the anode, in its region there is no more ban on the fulfillment of the inequality $nG\geq1$ (Vagner et al., 1974). Physically, this means that this inequality is valid when one or more electrons take part in generating one or several pairs of positive ions, thus providing conditions for a gas discharge outside the anode. The existence of the outside-electrode discharge suggests the conclusion that the discharge particles are in free motion (Vagner et al., 1974). This sharply reduces the impact of the discharge unit operation modes on the parameters of the particles,

practically eliminating the loading effect and cathode protection from sputtering. Free motion of the particles and sharp boundaries of the discharge suggest that outside the anode the particles move straight and perpendicularly to its surface. Actually, Fig. 3 shows that the distribution of the charged particles across the plasma flow is uniform, with its motion toward the sample surface being perpendicular.

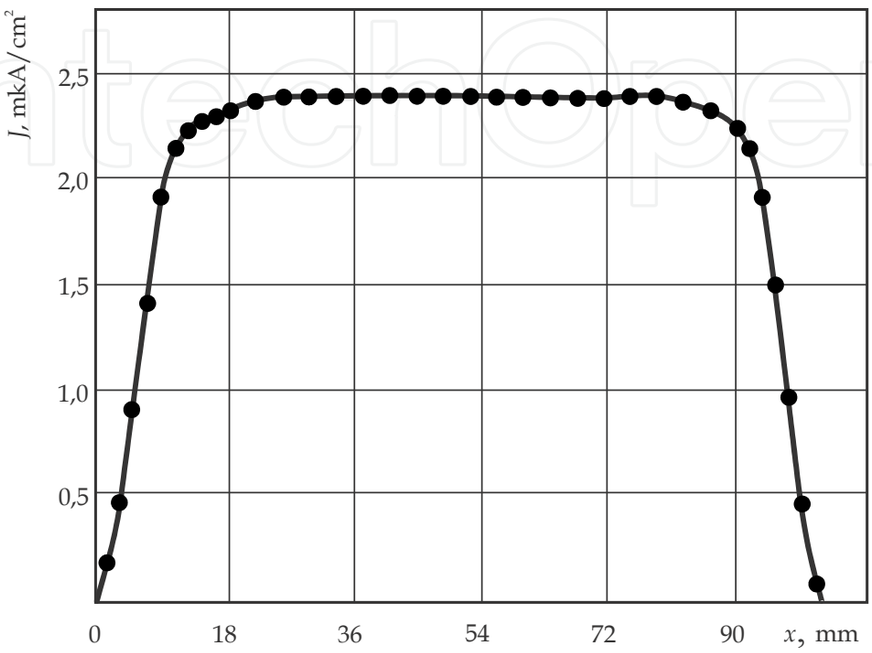

Fig. 3. Distribution of the charged particles across the plasma flux

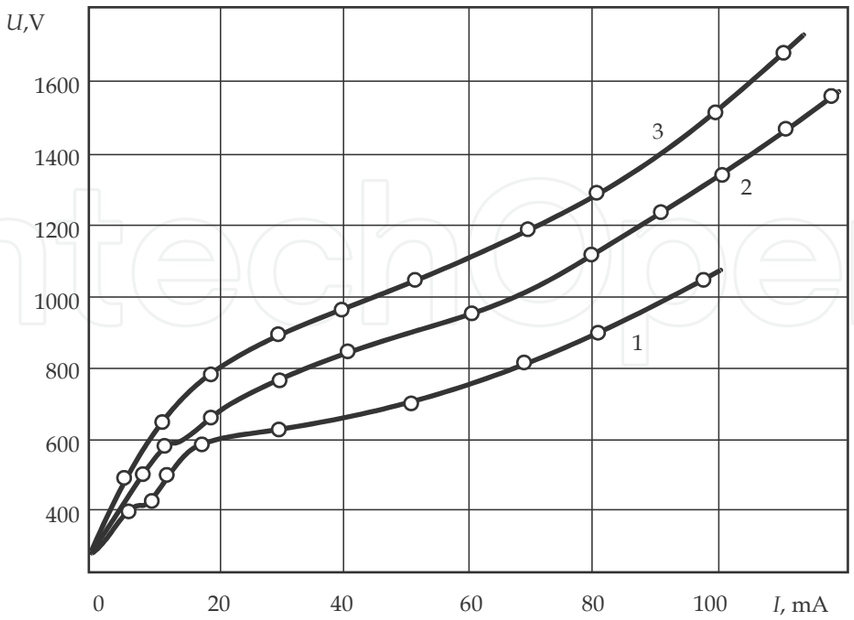

Fig. 4. The *V-I* curve of the high-voltage gas discharge at various pressures in the chamber: 1-1.5·10^{-1}torr; 2-1.2·10^{-1} torr; 3-9·10^{-2} torr.

Analysis of the *V-I* curve of the discharge (Fig. 4) shows that its formation is due to the ionization process of atoms of the working gas (*a* -process) and the cathode material (γ-process) (Chernetsky, 1969). It is noteworthy that in the range of voltages $300 \le U \le 1000$ V the working gas atoms ionization is predominant, whereas at $U \ge 1000$ V the intense cathode sputtering takes place, thus leading to the ion-electron emission responsible for the remaining section of the *V-I* curve.

However, in the region of relatively low pressure ($p \le 1.5 \cdot 10^{-1}$ torr), in the range $20 \le I \le 50$ mA, there is a pronounced *I-V* curve section where the *I*-dependence is weak. This suggests that for the above voltage range and high pressures, the electrons still manage to gain sufficient energies for the working gas atom ionization, thus actively contributing to the current increase even at a small voltage increase.

The assumption made is in good agreement with the plot shown in Fig. 5: the voltage saturation in the pressure range $1.8 \cdot 10^{-1}$ torr $\ge p \ge 9 \cdot 10^{-2}$ torr in the case of a clean (new) cathode proves that the working gas ionization capabilities have been exhausted, with sputtering and ionization of the cathode atoms (ion-electron emission) being responsible for the curve rise at $p < 9 \cdot 10^{-2}$ torr.

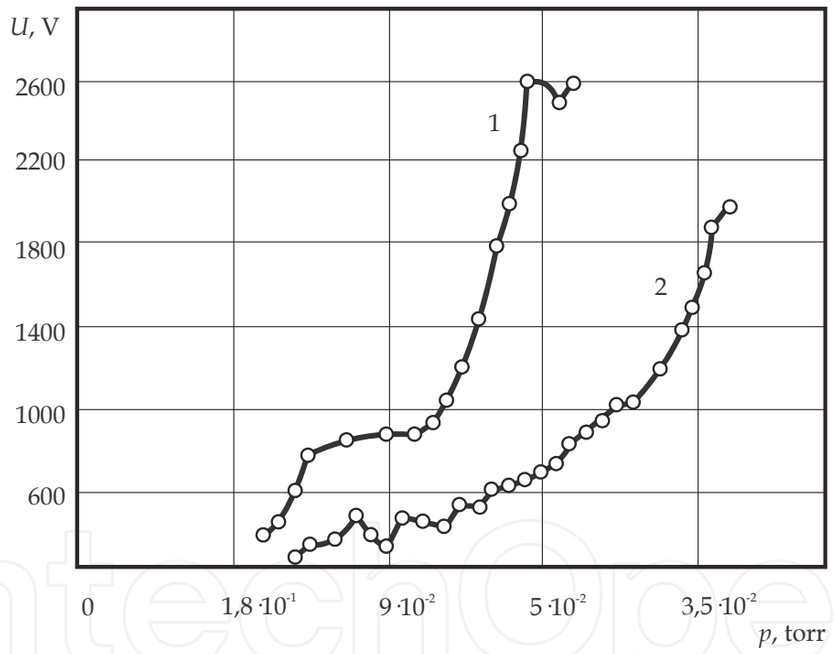

Fig. 5. The cathode voltage vs the chamber pressure: 1 - clean (new) cathode, 2 - contaminated cathode (after a long period of work)

To prove the above statements we will estimate the parameters of mechanisms that provide the gas discharge existence. It has been known that the ionization of the working gas atoms can result from the electron (*a*-process) and positive ion (β-process) action. The secondary electron emission can be caused by the ion bombardment (γ-process) and radiation-induced surface ionization (δ-process) (Chernetsky, 1969). Let us elucidate which of the above-listed processes are predominant in the emergence and maintenance of the high-voltage gas discharge.

The volume ionization coefficient that characterized the α-process is given by (Raizer, 1987)

$$a_i = \frac{1}{l_i} = \frac{E}{\varphi_i}, \tag{1}$$

where l_i is the ion range, cm, φ_i is the ionization potential, V, and E is the strength of the nonuniform electric field, V/cm, derived from the relation (Kolpakov & Rastegayev, 1979)

$$E(y) = \frac{4cU/\pi}{(1 + h/c\pi)\,4c^2 + y^2}, \tag{2}$$

where U is the cathode voltage, V, c is a constant derived from a set of equations (Kolpakov & Rastegayev, 1979), which equals c=0.08 cm for a 1.8 x 1.8 mm anode hole, and h is the cathode-to-anode distance, cm. To derive the strength of the electric field acting upon a charged particle at the first length of its free path λ, cm, we must replace y in (2) with the value of λ derived from

$$\lambda = \frac{4\sqrt{2}}{n_0 \sigma}, \tag{3}$$

where n_0 is the concentration of molecules of the hladon-14 gas, which equals n_0=0.29·10^{16} cm^{-3} for the pressure of 9·10^{-2} torr and σ is the effective cross-section of the chladon-14 molecule. According to the calculation based on Eq. (3), we find λ = 1.3 cm. Substituting the known discharge ignition voltage of U=300 V, as well as the h=0.5 cm and c=0.08 cm, into Eq. (2) we obtain E=15.4 V/cm. Substituting the derived value of the electric field strength into Eq. (1) yields a_i =1 cm^{-1}, which corresponds to the condition for the outside-anode gas discharge ($nG \geq 1$). Also, the comparison of the values of λ and l_i at the above voltage has shown that $\lambda > l_i$, suggesting the ionization possibility of the remaining gas molecules (Chernetsky, 1969).

The efficiency of the positive-ion-induced ionization of the working gas molecules is small and, therefore, the β-process can be disregarded when studying the gas discharge (Raizer, 1987). Because the high-voltage discharge is independent, with no extra irradiation sources found in the discharge vacuum camera, the δ-process can also be disregarded. Hence, the positive ions are the major source of cathode-emitted secondary electrons. The contribution of the positive ions to the production of the secondary electrons is characterized by the secondary emission coefficient, which equals γ=7.16·10^{-5} for U=300 V (Izmailov, 1939). Given the cathode voltage of 1000 V, the above-discussed calculation techniques give the following values of the coefficients (Izmailov, 1939): $a_i \approx 4{,}8$, $\gamma = 0{,}66$. From comparison of the two values, we can see that there is only a three-fold increase in the volume ionization of the working gas molecules, whereas the ionization due to ion-electron emission has increased by a factor of 10^4. Thus, for the cathode volume in the range $300 \leq U \leq 1000$ V the working gas ionization is mainly due to the volume ionization by electron impact. For $U \geq 1000$ V, the major ionization mechanism is ion-electron emission, which complies well with the plots shown in Figs. 2 and 3.

The violation of the exponential dependence in Fig. 3 in the range p= 5.5·10^{-2} -4.8·10^{-2} torr is due to emergence of unstable microarch discharges between the cathode and anode, seen with naked eye. The conditions for emergence of this type of parasite discharge in the above range of values and pressures become similar to those for the high-voltage discharge and, therefore, the two emerge practically simultaneously. With further increase of voltage, one

of the discharges starts to prevail, with a breakdown of the dielectric inter-electrode space ensuing. Traces of three such breakdowns are shown in Fig. 6.

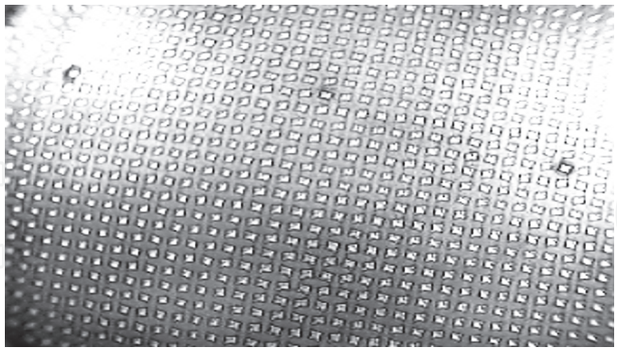

Fig. 6. Breakdown traces and general appearance of the cathode surface after a long period of work

The absence of saturation in the case of the contaminated cathode (Fig. 5, after a long period of work) suggests that there are structural changes on the cathode surface, as seen in Fig. 6. These appear in the course of operation under the action of plasma flow microrays, reproducing the contours of the anode holes. It has been known (Matare, 1974) that any disturbances of the crystalline lattice cause the interatomic bonds to be weakened. Such disturbances possess lower ionization potential due to ion bombardment compared with the core material, Thus as it would be expected, the potential of the high-voltage discharge ignition should be decreased, in accordance with the form of the curve in Fig. 5. In this case, the character of the curve is determined by the predominant emission of the cathode material, which begins at a lower pressure. Low pressure facilitates the elimination from the cathode surface of easily evaporated contamination particles, such as various atoms and molecules absorbed by the surface, leaving the ion-electron emission the only mechanism for maintaining the discharge.

Thus, for the cathode voltages in the range $3000 \leq U \leq 1000$ V the high-voltage discharge is mainly maintained with the α-process, whereas at $U \geq 1000$ V the discharge exists due to the γ-process.

4. Theoretical and experimental investigation of surface treatment mechanisms with the directed flows of the off-electrode plasma

In particular, (V.A. Kolpakov, 2002) has shown that high-voltage gas discharge is in principle suitable for plasma etching and reactive ion etching. At the same time, we are unaware of current reports in which the mechanism of surface treatment with the directed flows of the off-electrode plasma is explored in a practical context.

The aim of this part was to investigate surface treatment mechanisms with the directed flows of the off-electrode plasma. The process was applied to SiO_2 and also some other materials, widely used in micro-, nanoelectronics and diffractive optics.

4.1 Basic reactions in plasma etching and reactive ion etching by the off-electrode plasma

Kolpakov (V.A. Kolpakov, 2002) has shown that high-voltage gas discharge can provide plasma etching or reactive ion etching, depending on the applied voltage or the cathode–

wafer spacing. With plasma etching, the wafer is bombarded by normally incident ions. This feature enhances etching anisotropy and increases the etch rate, because the reactive species, such as atomic fluorine, are produced just on the wafer surface. The species are formed by interaction between negative ions and adsorbed neutral process-gas molecules.

Ion bombardment is the main source of reactive species in plasma etching. To show this, we examine plasma reactions in the case of CF_4. With radio-frequency or microwave discharge, reactive species, namely, F^* radicals, can be produced both in the bulk of the plasma and at the wafer surface by electron impact dissociation of neutral molecules (Flamm, 1979):

$$e^- + CF_4 \rightarrow CF_3^+ + F^* + 2e^-, \tag{4}$$

$$e^- + CF_4 \rightarrow CF_3^* + F^* + e^- , \tag{5}$$

$$e^- + CF_4 \rightarrow CF_3^* + F^- . \tag{6}$$

It appears reasonable to say that high-voltage gas discharge is an anomalous form of glow discharge. If the spacing between a solid anode and a cathode is reduced to the Aston dark space, the glow discharge will disappear, because $nG < 1$, where n and G are the respective densities of electrons (negative ions) and positive ions. If, however, an aperture is made in the anode, then we shall have $nG \geq 1$ near the aperture (Vagner et al., 1974). Gas discharge will thus arise at a certain distance from the anode. In high-voltage gas discharge, therefore, charged particles are strongly separated according to the sign of the charge: an as-produced negative ion or electron will move toward the wafer, while the corresponding positive ion will be heading toward the cathode. An interaction event may also yield two or more negatively charged particles (ions and/or electrons), but at the same time it must generate an appropriate number of positive ions in order to maintain charge equilibrium: $nG \geq 1$. If this condition is not fulfilled in a region, high-voltage gas discharge will cease to exist there. This occurs where the energy of negatively charged particles is too low to allow production of positive ions in collisions with process-gas molecules, as in regions outside the output stream of the plasma source (V.A. Kolpakov, 2002). In this respect, reaction (4) is the best, giving a ion. It has been emphasized that in the voltage range 0.5–2 kV electrons are lost mainly due to their capture by neutral atoms (V.A. Kolpakov, 2002). In particular, this is true of the plasma etching mode. The lifetime of reactive species is short at the voltages. The free radicals F^* decay as

$$F^* + e^- + e^- \rightarrow F^- + e^- . \tag{7}$$

Since high-voltage gas discharge produces a plasma stream, the particles rarely collide with the wall, so that wall recombination can be neglected when examining the plasma processes. Electron–ion recombination requires that, aside from an adequate density of free electrons, their energies be less than the ion ionization potential. As these conditions are not fulfilled in the plasma etching mode, charge neutralization is mainly by ion–ion recombination (Raizer, 1987). In addition to electron–ion recombination, we exclude electron-impact excitation and ionization of process gas molecules, because these effects can occur at a higher pressure (Chernyaev, 1987; Ivanovskii, 1986). Thus, the above considerations allow the following main reactions in the bulk of an high-voltage gas discharge plasma:

$$e^- + CF_4 \rightarrow CF_3^+ + F^- + e^- \tag{8}$$

$$F^- + CF_4 \rightarrow CF_3^+ + 2F^- \tag{9}$$

$$F^- + CF_3^+ \rightarrow CF_4 . \tag{10}$$

Reaction (9) is possible because the energy E of F^- ions was found to exceed the ionization potential of CF_4 throughout their progress toward the wafer, as follows from the equation

$$E_n = E_{n-1}(1-\gamma) + \Delta U_n , \tag{11}$$

where ΔU_n is the accelerating potential difference after the corresponding collision and $\gamma = 4mM/(m+M)^2$, with m and M denoting the respective masses of an ion and a process-gas molecule (V.A. Kolpakov, 2002). We calculated that E should decrease from 400 eV just after a first collision to below 100 eV just before the collision with a CF_4 molecule adsorbed by the wafer. In the last collision a proportion of the ion energy (on the order of the ionization potential) is consumed by the ionization of the molecule, and the rest goes into the breakage or weakening of bonds between the atoms of SiO_2 molecules on the wafer surface. The collision produces free radicals by the equation

$$F^- + CF_4 + S_s \rightarrow CF_3^+ + 2F^* + 2e^- , \tag{12}$$

where S_s denotes a surface species. As-generated radicals react with SiO_2 to form volatile substances:

$$4F^* + SiO_2 \rightarrow SiF_4 \uparrow + O_2 \uparrow . \tag{13}$$

We see that every F^- ion generated in the bulk of the plasma creates a radical on the wafer surface, the reaction products being withdrawn from the work chamber. If a collision occurs between an F^- and a CF_3^+ ion such that the energy of the former is less than or equal to the ionization potential of the latter, the two ions recombine to produce a CF_4 molecule according to (10).

Thus, for high-voltage gas discharge (off-electrode) plasma etching, Eqs. (8)–(10), (12), and (13) imply the following advantages: (i) Reactive species are formed exactly on the wafer surface; therefore, they cannot decay by interaction with other plasma particles. (ii) F^- ions (due to ionization of CF_4) play the major part in the production of reactive species. (iii) The collision between an F^- ion and a process-gas molecule adsorbed on the SiO_2 surface yields two reactive species, the surface serving as a catalyst. (iiii) There is no carbon deposition on the wafer surface, because CF_3^+ ions are attracted by the cathode and so cannot produce $(C_xF_y)_n$ polymers on the surface (Fig. 1a).

In the reactive ion etching mode of treatment with CF_4 plasmas, the energy of F^- ions incident on the SiO_2 surface is so high (100–500 eV) as to strongly heat the surface. This impedes process-gas adsorption and hence virtually prevents reactive species from taking part in etching (Kireev et al., 1986; V.A. Kolpakov, 2002). Erosion is due to sputtering by F^-

ions and their reaction with the sputtered matter. Reactions in this case are similar to those in the plasma etching mode. Also note that the mechanism of reactive ion etching is extensively treated in the literature (Ivanovskii, 1986). We therefore shall not address reactive ion etching with pure CF_4 in the subsequent text.

Far more interesting is the high-voltage gas discharge etching in which CF_4 is mixed with O_2. Guided by the discussion above, we can reasonably expect that aside from reactions (8)–(10) the plasma will exhibit

$$e^- + O_2 \rightarrow O^+ + O^- + e^- , \tag{14}$$

$$e^- + OF \rightarrow O^+ + F^- + e^- , \tag{15}$$

$$F^- + O_2 \rightarrow O^+ + O^- + F^- , \tag{16}$$

$$F^- + OF \rightarrow O^+ + 2F^- , \tag{17}$$

$$O^- + CF_4 \rightarrow CF_3^+ + F^- + O^- , \tag{18}$$

$$O^+ + F^- \rightarrow OF , \tag{19}$$

$$CF_3^+ + O^- \rightarrow COF_2 \uparrow + F^* \tag{20}$$

Reactions (14)–(17) occur under ionization, while reactions (19) and (20) under recombination.

Furthermore, it has been noted that the volatile product, COF_2, decomposes to give free fluorine radicals (Gerlach-Meyer, 1981):

$$COF_2 \rightarrow CO \uparrow + 2F^* . \tag{21}$$

Finally, an F^* atom can capture an electron by Eq. (7) to become an F^- ion, and this in turn can take part in plasma etching, producing F^* according to Eq. (12). It appears reasonable to expect that O^- ions will undergo similar transformations, with the result that oxygen radicals will compete with F^* radicals for active sites on the SiO_2 surface. This factor is likely to reduce the rate of plasma etching at certain O_2 concentrations.

4.2 Results and discussion: etch rate in relation to oxygen percentage and other process parameters

To optimize the etch rate in CF_4–O_2 plasmas, it is important to know how it varies with oxygen percentage. Let us first consider the plasma etching mode of treatment. Figure 7a shows graphs of the dependence measured for different discharge currents. Notice that with increasing oxygen percentage the etch rate first rises and then falls to almost zero values. The graphs are similar in shape for all the discharge currents except the minimum one, 50 mA. For this current the insignificant variation in etch rate is attributable to a low density of charged particles in the plasma: with a low ionization rate of process-gas molecules by O^-

ions, these make a modest contribution to the production of F^- ions (see Eqs. (18), (20), and (21)). With pure CF_4, etching was not observed at the minimum discharge current.

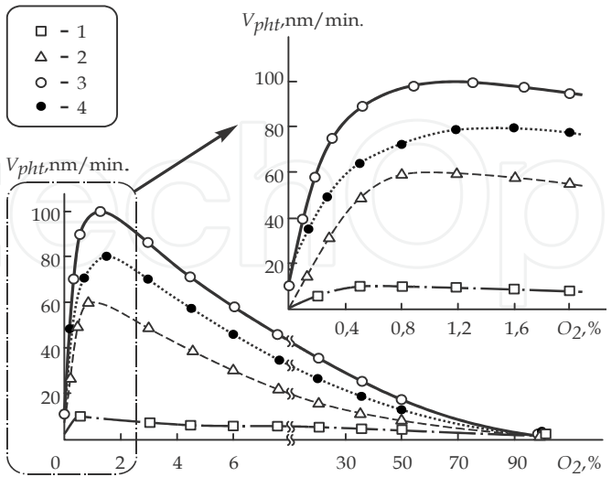

(a)

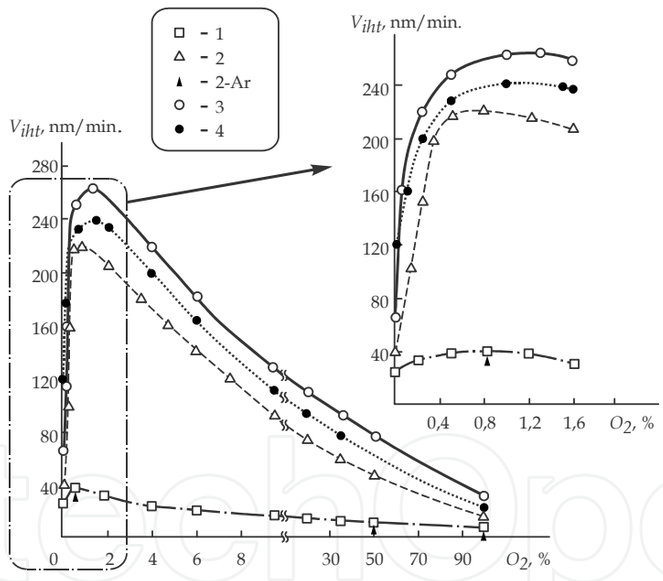

(b)

Fig. 7. Etch rate vs. oxygen percentage in (a) the plasma etching and (b) the reactive ion etching mode of treatment at discharge currents of (1) 50, (2) 80, (3) 120, and (4) 140 mA. The cathode voltage is (a) 0.8 or (b) 2 kV

The effect of discharge-current variation on the etch-rate pattern can be explained as follows. As the discharge current increases, so should do the density of charged particles in the plasma. This in turn should increase the ionization rate of CF_4 molecules by O^- ions and hence the density of F^- ions produced with the assistance of oxygen.

The steep, rising segments of curves in Fig. 7a should indicate deficiency in F^* radicals at the wafer surface, implying that etch rate is determined by the density of F^- ions. The pronounced peak, observed at each discharge current, should correspond to the situation in which all of the oxygen takes part in the production of F^- ions; at the same time, the oxygen does not compete with F^* radicals for active sites on the SiO_2 surface, nor does it passivate the surface. It is important to note that the etch rate peaks for an oxygen percentage as low as 0.5–1.5%. This finding must indicate high transverse uniformity of the plasma stream, its normal incidence on the wafer surface, and freedom from wall collisions. Also, every O^- ion produced in the bulk of the plasma by Eqs. (14) and (16) must be involved in the generation of an F^- ion, which in turn will create reactive species:

$$O_2 \xrightarrow{e,F^-} O^- \xrightarrow{CF_4} F^- \xrightarrow{S_S} F^* .$$

The falling segments of the etch-rate graphs should be due to occupation of vacant SiO_2 bonds by oxygen radicals, which thus compete with fluorine ones. Further, oxygen molecules excited at the SiO_2, surface should react with F^* radicals to convert them into F_2, a less reactive substance (Harsberger & Porter, 1979). The density of reactive species is thus reduced. When the plasma is generated in pure oxygen, the SiO_2 surface is fully passivated, so that the etch rate is close to zero; this conclusion is consistent with the established conception (Chernyaev, 1987; Ivanovskii, 1986; Kireyev & Danilin, 1983).

Let us now turn to the reactive ion etching mode of treatment. The corresponding etch-rate curves are shown in Fig. 7b. The etch rate also rises with oxygen percentage while the latter is not too high. However, such behavior in the reactive ion etching case is at variance with long-standing views (Horiike, 1983; Ivanovskii, 1986). To clarify the point, let us examine Fig. 7b. On the whole, the etch rate follows the same pattern as in the plasma etching case. This is obviously attributable to the fact that only neutral process-gas molecules and charged plasma particles are in the bulk of the plasma. Fluorocarbon and oxygen ions are unlikely to combine into stable molecules (CO, CO_2, and COF_2) on account of the above-mentioned separation of charged particles and the action of a strong, nonuniform electric field (Kolpakov & Rastegayev, 1979; V.A. Kolpakov, 2002). Consequently, high-energy O^- and F^- ions produced in the plasma stream (see Eqs. (14)–(18)) should not recombine as they travel toward the wafer. These ions will erode the material first by sputtering and then by chemical reactions. In the sputtering, highenergy ions penetrate a certain depth into the material and in doing so break interatomic bonds. Having lost energy, the ions can interact with the material only by chemical reactions. As with plasma etching, this stage of reactive ion etching is characterized by competition between reactive fluorine and oxygen species for active sites; however, these are now located in the bulk of SiO_2. This explains why the etch rate starts falling once the oxygen percentage has reached 1.5%. Also, the etch rate does not vanish, however high the oxygen percentage is, implying that pureoxygen etching occurs by sputtering with O^- ions. In fact, this mechanism starts acting at an oxygen percentage of 10%. It is manifested in characteristic dips in the etching profile (Orlikovskiy, 1999a), as shown in Fig. 8, which indicate that reevaporation rather than chemical erosion dominates the sputtering (Chernyaev, 1987).

Comparing Figs. 7a and 7b, we notice that the etch rate peaks for the same oxygen percentage. This fact is evidence that in plasma etching and reactive ion etching the same

processes occur in the bulk of the plasma (or at least upstream of the wafer), thus supporting the mechanisms and equations proposed above. Otherwise, the etch rate would decrease at low oxygen percentages. The nonzero etch rate at zero oxygen percentage, observed even at a discharge current as low as 50 mA, signifies that the voltage between the electrodes is the major factor in the transport of reactive species to the wafer. The higher rate of change shown by the reactive ion etching curves should be due to sputtering.

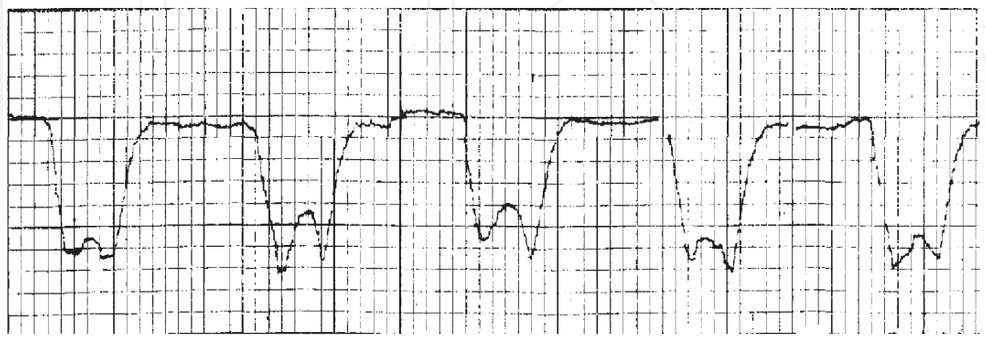

Fig. 8. Reactive ion etching trench profile obtained at an oxygen percentage above 10%. The horizontal and the vertical scale read to 2 and 0.2 μm, respectively

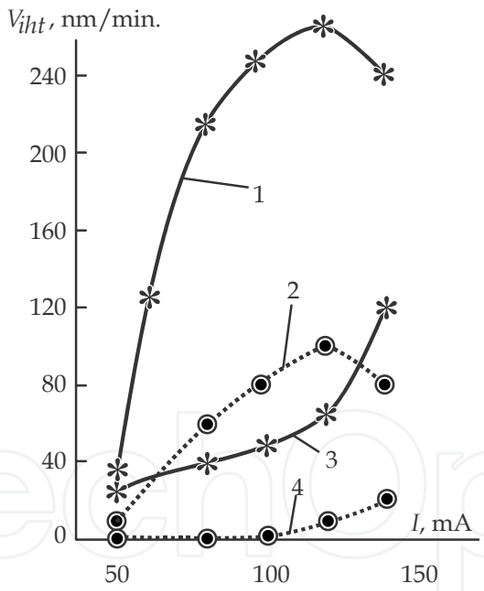

Fig. 9. Etch rate vs. discharge current for (1, 3) reactive ion etching or (2, 4) plasma etching in (1, 2) a CF_4–O_2 or (3, 4) a CF_4 plasma

It was found that addition of oxygen to CF_4 is most effective if the discharge current is in the range 80–120 mA, for both modes of etching (Fig. 7; Fig. 9, curves 1, 2). If the current is increased further, the etch rate falls because the large density of reactive species on the wafer surface makes it difficult to remove etch products. The removal is therefore the rate-determining factor. This conclusion is supported by etch-rate curves 3 and 4 of Fig. 9. These show consistent exponential growth, indicating deficiency of reactive species on the SiO_2 surface. Thus, the etch rate in a CF_4 plasma is determined by the density of F^- ions produced

in the plasma, for both modes of etching. It was also observed that discharge currents above 140 mA cause high-temperature breakdown of the photoresist.

4.3 Effect of bulk modification of polymers in a directional off-electrode plasma flow

The treatment of polymers by low-temperature plasma is one of fundamental processes in preparing micro- and nanostructures. The regularities of this technological process have been studied for a long time (Moreau, 1988a; Sarychev, 1992; Valiev et al., 1985, 1987). However, in spite of the large number and apparent comprehensiveness of available experimental results, the mechanism of polymer etching is not completely clear in view of its complex multifactor dependence on the type of interaction of active particles in the plasma with the polymer matrix.

This part of chapter is devoted to experimental investigation of regularities of polymer etching in the plasma generated outside the electrode gap in oxygen. The experimental results are used for constructing a computational model of the etching process.

Figure 10 shows the experimental dependences of the thickness of etched polymer layer (h) on etching time (t) for two different values of the initial film thickness. Analysis of these dependences shows that both curve display identical behavior in the region $0 \le t \le 18$ s: the value of h increases for $0 \le t \le 6$ s and $15 \le t \le 18$ s ($15 \le t \le 21$ s for curve 1) and the rate of etching decreases for $6 \le t \le 15$ s. Both curves have regions of saturation for values of h equal to the corresponding values of the film thickness, which confirms the complete removal of polymer from the surface.

Let us use the experimental results for constructing the model of polymer etching in the oxygen plasma outside the electrode gap.

It should be noted that the most comprehensive mechanisms and models of polymer etching in the high-frequency and ultrahigh-frequency (microwave) plasma were proposed in (Sarychev, 1992; Valiev et al., 1985, 1987). It was assumed that a modified surface layer (K-layer) is formed during etching, which is more resistive to destruction than unmodified lower layers of the polymer structure.

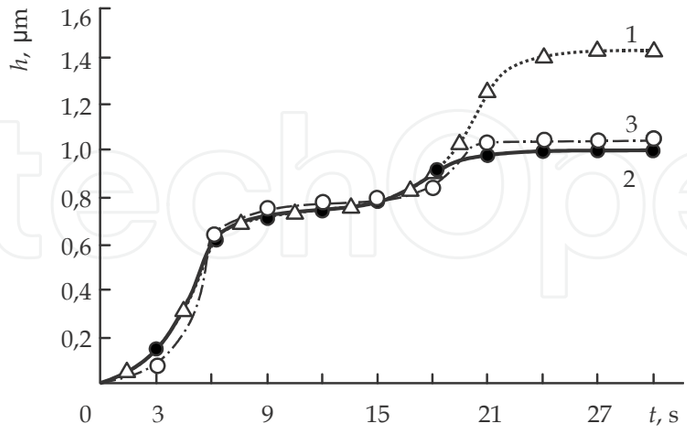

Fig. 10. Dependence of the thickness of the scoured polymer layer on the etching time for I = 100 mA and U = 2 kV: 1—initial thickness of polymer film is $1.4 \cdot 10^{-6}$ m; 2—$1 \cdot 10^{-6}$ m; 3—calculated dependence for an initial thickness of the polymer film of $1 \cdot 10^{-6}$ m

It should be noted, however, that the model of K-layer was developed on the basis of experiments on etching in the electrode plasma. Interpretation of our results on etching

outside the electrode gap allows us to supplement this model by the idea that the modified layer in this case may lie in the bulk of the polymer.

In an oxygen plasma, atomic oxygen (O^{**}), negative oxygen ions (O^-), and excited molecular oxygen (O_2^*) with a low concentration on the order of 0.01% are active etching particles (Ivanovskii, 1986). Polymer etching may occur due to sputtering by high-energy O^- ions, as well as due to their chemical interaction with polymer molecules. In addition, atomic oxygen O^{**} present at the surface can also interact with these molecules. The reaction products form volatile compounds H_2O (water vapor), CO_2, and N_xO_y, which are removed from the working chamber by evacuation facilities.

The role of electrons in this process is controlled by the following circumstance. The electron mean free path in the gas and in the polymer is much larger than the mean free path of an ion due to smaller number of collisions with atoms and molecules of the medium. Electrons penetrate to the bulk of the polymer to a depth (Rykalin et al., 1978)

$$L = 10^{-5}\frac{U^{3/2}}{\rho}, \tag{22}$$

where ρ = 500 kg/m^3 is the polymer density; U = 2 kV is the accelerating voltage; and L = 0.57·10^{-6} m, which is half the thickness of the polymer film and in good agreement with experimental curve 2 (see Fig. 10). Electrons are decelerated in the substance due to excitation of atoms in polymer molecules. In each collision, an electron spends for excitation an energy (Raizer, 1987)

$$\varepsilon = \frac{2m_e}{M}E_e, \tag{23}$$

where M is the mass of an atom in a polymer molecule and E_e is the initial energy of the electron. For E_e = 2000 eV, the value of $\varepsilon \approx 0.005$ eV, which is several orders of magnitude lower than the ionization loss. The electron energy loss distribution over the path depth in this case can be described by the Thomson—Widdington law (Popov, 1967). An electron experiences about 30 collisions over length L; in this case, it releases an energy of 1.9 keV at the end of its path, spending this energy for rupture of bonds between atoms in the polymer layer.

As a result of excitation, polymers may experience relaxation, which is observed at temperatures equal to or exceeding the glass-transition temperature T_s (Bartenev & Barteneva, 1992). For a DNQ protecting layer obtained from metacresol novolac, T_s = 423 K (Moreau, 1988a); consequently, relaxation does not take place. Hence, the increase in the dependences on segment $0 \le t \le 6$ s can be explained by the interaction of active plasma particles with excited polymer atoms, for which the number of active bonds N_a is determined by the flux of electrons, their energy E_e, and duration t of the process.

When the rupture of atomic bonds takes place, atoms containing a single uncompensated electron each on the outer orbital try to fill it. Bonds involving the collectivization of electron pairs are formed between adjacent carbon atoms.

Thus, a modified layer consisting predominantly of carbon atoms is formed at a depth L. This layer must possess an elevated density ρ_m (as compared to unmodified layers) and stability to destruction (Valiev et al., 1985). The degree of homogeneity of this layer depends on the uniformity of the distribution of charged particles over the plasma flow cross section,

the dose and energy of electron irradiation recalculated for the number of carbon atoms in the layer with different numbers of ruptured (suppressed) bonds and, accordingly, with different degrees of modification (Fig. 11a).
Such a mechanism explains the existence of two first regions for $0 < t < 6$ s and $6 < t < 15$ s of curve 1 in Fig. 10.
For $15 \le t \le 21$ s, curve 1 (see Fig. 10) has a second segment in the dependence of $h = f(t)$, indicating the etching of a material with properties close to initial properties. Let us consider the mechanism of its formation.

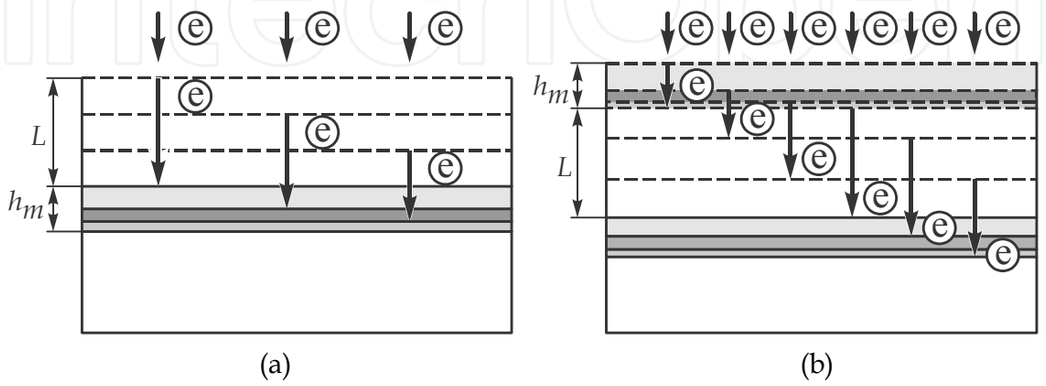

Fig. 11. Diagram illustrating the formation of a modified layer by electrons: (a) polymer etching stage with initial properties; (b) modified polymer layer etching

The motion of electrons in a denser medium is accompanied by their scattering, which is proportional to the mean free path. In the course of etching of a layer of modified polymer, the mean free path decreases, which increases the electron flux and energy (ΔE_e) carried by the electron flow to the lower (unmodified) region. This becomes possible if the etching rate V_m in the modified layer exceeds the rate V of its formation. In this case, if condition $\Delta E_e \ge E_{thr}$ is satisfied (E_{thr} is the threshold energy of delocalization, which is a part of the binding energy (Bechstedt & Enderlein, 1988), a new stage of formation of layers with different degrees of modification begins (it includes the stage of excitation of atoms) (Fig. 11b). The number of such layers is proportional to the thickness of the polymer film. The correctness of the above statements follows from experimental curve 1 (see Fig. 10). Indeed, this curve clearly displays the second peak corresponding to the stage of formation of the second modified layer.
Thus, the process of polymer removal consists of two stages: etching of unmodified and modified layers. The second stage for an individual region of the polymer lags behind the first stage by t_m, where t_m is the etching time for the unmodified polymer.
Let us estimate the height h of the etched layer as a function of parameters of the physical process (discharge current, accelerating voltage, and duration of etching) on the basis of the proposed mechanism and experimental results. The value of h is

$$h = \sum_{n=0}^{l-1} \left[\int_{nT}^{t_m+nT} V_0(t)\,dt + \int_{t_m+nT}^{(n+1)T} V_m(t)\,dt \right], \tag{24}$$

where $T = t_m + t_k$ (t_k is the time of etching of modified polymer); $n = 0, 1, 2, \ldots, l - 1$ (l is the number of modified layers); and t is the etching time. Considering that excitation of polymer

atoms increases the etching rate, while the decrease in this rate is due to rupture (suppression) of bonds in the polymer at depth L, we can write

$$V_0(t) = V_0 \frac{N_a(t)}{N_{sn}} \; ; \; V_m(t) = V_m\left(1 - \frac{N(t)}{N_{sm}}\right), \tag{25}$$

where N_{sn} and N_{sm} are the total number of bonds in unmodified and modified layers of thickness L and h_m, N is the number of ruptures (suppressed) bonds, and V_0 and V_m are the etching rates for the polymer and the modified layer in the high-voltage gas discharge plasma flow (V.A. Kolpakov, 2002):

$$V_0 = \frac{BM}{\rho N_a} J_i^- \left|\exp\left(\frac{U - U_{gr}}{U}\right) - 1\right| \left(k_1 + k_3\right), \tag{26}$$

$$V_m = \frac{BM}{\rho_m N_a} J_i^- \left|\exp\left(\frac{U - U_{gr}}{U}\right) - 1\right| \left(k_1^m + k_3^m\right), \tag{27}$$

$$J_i^- = \left(1 - \frac{d}{d_{\max}}\right) \frac{I}{qeS_K} \left(1 - \frac{\gamma_e \eta}{(1+\gamma_e)} \exp\left[(a - a_n) d_{\max}\right]\right), \tag{28}$$

where N_a is the Avogadro number, k_1 and k_1^m are the plasma-chemical etching coefficients, equal to the number of polymer atoms of unmodified and modified layers removed by a chemically active particle; k_3 and k_3^m are the physical sputtering coefficients equal to the number of atoms knocked from the surface of unmodified and modified layers by a bombarding particle; U_{gr} is the voltage across the gas discharge unit, for which the energy of an ion at the instant of its approach to the surface of treatment is at the threshold energies of plasma-chemical and ion-chemical etching; B is the (constant) value of the penalty function obtained from the natural experiment, which is $B \approx 0.6$ for $I = 100$ mA (V.A. Kolpakov, 2004); $d = 0.045$ m is the distance from the cathode to the sample surface; $d_{\max}$ is the maximal distance over which the plasma flow propagates for the given voltage across the electrodes; S_K is the surface area of the cathode; q is the geometrical transparency of the gauze anode; γ_e is the secondary emission coefficient; η is the electron beam focusing coefficient; a is the ionization factor; and a_n is the adhesion coefficient.

Having analyzed the nature of variation of experimental curves on segment $0 \le t \le 6$ s (see Fig. 10) and the above statement concerning the dependence of N_a on the electron flux and energy, as well as on the duration of the process, we approximate $N_a = f(J_e, E_e, t)$ by an exponential function of the form

$$N_a(t) = N_0 \exp\left(\frac{J_e S E_e}{E^*} t\right), \tag{29}$$

where N_0 is the number of bonds on the polymer surface (on the order of 10^{16}), $E^* = N_{sn} E_{thr}^*$ is the total energy required for exciting polymer atoms in a layer of thickness is the

threshold energy of excitation of a polymer atom, J_e is the electron flux, S is the area of interaction of the low-temperature plasma with the polymer, and E_e is the electron energy.
Analysis of the structure of the DNQ protecting material based on diazoquinone and metacreson novolac leads to the conclusion that carbon is the main bond-forming element. Knowing the number of carbon atoms n_C in a polymer molecule and its valence V_C, as well as the total number of atoms n_{at} in a polymer molecule, we can estimate quantities N_{sn} and N_{sm} from the formula

$$N_{sn} = \left(V_C n_C\right)\frac{\rho S}{M}\frac{N_A}{n_{at}}L\,,$$

$$N_{sm} = \frac{N_{sn}}{L}h_m \;;\; h_m = 10^{-5}\frac{U^{3/2}}{\rho_m}\;. \tag{30}$$

Substituting the known values of n_C = 47, V_C = 4, and n_{at} = 108 into these formulas, we obtain $N_{sn} \approx 0.4 \cdot 10^{18}$ and $N_{sm} \approx 0.16 \cdot 10^{18}$. The energy released by an electron at the end on its path in the polymer for rupturing (suppression) of bonds is controlled by difference $E_e - E^*$, where E^* is the total energy spent by the electron for excitation of polymer atoms. In this case, quantity N can be represented analogously to relation (29) in the form

$$N(t) = N_0 \exp\left(\frac{J_e S}{N_{sm}}\frac{\left(E_e - E^*\right)}{E_{thr}}t\right). \tag{31}$$

In the time interval $0 \le t \le t_m$, etching of the polymer with initial properties takes place; as a result, k_1^m , $k_3^m = 0$ and the second term in relation (24) vanishes. The thickness of the scoured layer is proportional to the number of active bonds of excited polymer atoms. Ratio N_a/N_{sn} specifies the law of variation of the value of h on segment $0 \le t \le 6$ s in the dependence $h = f(t)$ depicted in Fig. 10. However, modified layers with various degrees of modification are formed at a depth $h \ge L$. By instant $t = t_m$ for which the number of active bonds becomes equal to the number of bonds in the unmodified layer ($N_a = N_{sn}$), etching of the unmodified polymer is completed, which leads to zero values of k_1 and k_3. For $6 \le t \le 15$ s, polymer layers with various degrees of modification experience etching; an increase in N slows down this process, which does not contradict the above mechanism. The law of variation of the value of h at a given segment of curve $h = f(t)$ specifies ratio N/N_{sm} subtracted from unity. The instant corresponding to completion of etching of the modified layer is determined by the equality $N = N_{sm}$, which leads to vanishing of the second term in relation (24). Alternation of the conditions for completion of etching of the modified and unmodified layers in time at the instant when these conditions hold makes it possible to use expression (24) for estimating the value of h for an arbitrary thickness of the polymer film for the given values of the discharge current, accelerating voltage, and t.
To obtain numerical values of N_a and N and, accordingly, the thickness of the scoured layer after the substitution of expressions (25) into (24), we must know the threshold values of excitation energy, delocalization energy, and the total energy spent by an electron for exciting polymer atoms. The results of computer and natural experiments lead to the

conclusion that the calculated dependence approximates experimental curve 2 (see Fig. 10) if $E^*_{thr} \approx 0.005$ eV, $E_{thr} \approx 0.015$ eV; in this case, the value of E^* varies from 10^3 eV to zero, which can be explained by the decrease in the electron mean free path in an unmodified polymer during its etching. The above values of E^*_{thr} and E_{thr} are two or three orders of magnitude lower than the ionization energy and satisfy the inequality $E^*_{thr} < E_{thr} < E_b$ (where E_b is the binding energy), which does not contradict the physical process and the firm opinion of the authors of (Bechstedt & Enderlein, 1988).

Our theoretical and experimental results which were obtained early allow to propose an analytical method of calculating the temperature of the surface exposed to an off-electrode plasma flux.

5. Temperature measurement of a surface exposed to an off-electrode plasma flux

At the present time, numerical methods of calculation are finding wide application in the theory of heat transfer. Indeed, the problem we are interested in can be viewed as the boundary-value problem inverse to the problem of heat conduction. In this case, taking measurements on one part of the surface, one can recover the heat load on other parts inaccessible to measurements. However, such an inverse problem of mathematical physics belongs to the class of ill-posed problems (Tikhonov & Arsenin, 1977); therefore, even an approximate solution can be obtained only with special numerical methods (Alifanov, 1983; Vabishchevich & Pulatov, 1986) providing its stability. At the same time, recent advances in the field of plasma physics make it possible to quantitatively evaluate the effect of the plasma in the form of a heat flux. Therefore, the problem of determining the sample temperature is suggested to be reduced to the analytical solution of the direct problem of heat conduction with mixed boundary conditions.

The charged particles of a plasma flux are uniformly distributed over its cross section in the region where they impinge upon the substrate surface (Kolpakov & V.A. Kolpakov, 1999). With this in mind and taking into account the geometry of the substrate and its single-crystal structure, one can use the heat conduction equation for the one-dimensional case (Samarskii & Vabishchevich, 1996) with the following boundary and initial conditions:

$$\begin{cases} T(x,0) = T_0 \\ T(b,t) = T_{low}(t). \\ q(0,t) = q_1 \end{cases} \tag{32}$$

As far as we know, analytical solutions to the heat conduction equation with conditions (32) are absent. Therefore, we take the most appropriate known solution to this equation with similar boundary and initial conditions (Alifanov, 1994),

$$T(x,t) = \int_0^t q_1(\varepsilon) \frac{\partial \theta(x, t-\varepsilon)}{\partial t} d\varepsilon + \int_0^t q_2(\varepsilon) \frac{\partial \theta(b-x, t-\varepsilon)}{\partial t} d\varepsilon + T_0, \tag{33}$$

where $q_1(\varepsilon)$ is the specific heat flux incident on the front surface $x = 0$ and $q_2(\varepsilon)$ is the specific heat flux carried away from the back surface of the sample. Function $\theta(x,t)$, the temperature

response of the body to the unit heat flux incident on one of the boundaries, is given by (Carslaw & Jaeger, 1956)

$$\theta(x,t)=\frac{1}{\lambda}\left\{\frac{at}{b}+\frac{3(b-x)^2-b^2}{6b}+\frac{2b}{\pi^2}\sum_{k=1}^{\infty}\frac{(-1)^{k+1}}{k^2}\exp\left(-k^2\pi^2\frac{at}{b^2}\right)\cos\left(k\pi\frac{b-x}{b}\right)\right\}, \quad (34)$$

Where b is the sample thickness, $a=\lambda/C$ is the thermal diffusivity, λ is the thermal conductivity, and C is the heat capacity per unit volume.
The form of function $q_1(\varepsilon)$ can be found by measuring the temperature of the back (lower) surface of the sample, $T(b,t) = T_{low}(t)$, with incident heat flux $q_1(\varepsilon)$ known. In this case, temperature $T(0,t)$ of the upper (exposed) surface is a partial solution to initial equation (33) and depends on $q_1(\varepsilon)$ and calculated value of $q_2(\varepsilon)$.
Using the Laplace transformation,

$$F(p)=\int_0^{\infty} f(t)\exp(-pt)\,dt, \quad (35)$$

we represent the left-hand side of Eq. (33) as a function of complex variable p,

$$T_{low}(p)\leftarrow T(b,t)\ . \quad (36)$$

The convergence condition imposed on integral (35) implies the need for finite approximation of the sum in (34). Expression (34) is known to be a convergent alternate series (Tikhonov & Samarskii, 1964); therefore, the sum can be calculated with a desired accuracy by discarding the right-hand part, the approximation error being no more than the absolute value of the first of discarded terms.
Let us transform the right-hand side of (33) by applying the convolution theorem (Ditkin & Prudnikov, 1966), which allows one to determine the original of the product of images,

$$T_0+\int_0^t q_1(\varepsilon)\frac{\partial\theta(x,t-\varepsilon)}{\partial t}d\varepsilon+\int_0^t q_2(\varepsilon)\frac{\partial\theta(b-x,t-\varepsilon)}{\partial t}d\varepsilon\leftarrow T_0(p)+Q_1(p)K_1(p)+Q_2(p)K_2(p), \quad (37)$$

where $T_0(p)$, $Q_1(p)$, and $Q_2(p)$ are the images of initial temperature T_0, heat flux $q_1(\varepsilon)$, and heat flux $q_2(\varepsilon)$, respectively, and $K_1(p)$ and $K_2(p)$ are the images of the time derivatives of temperature responses $\theta(b,t)$ and $\theta(0,t)$, respectively,

$$\begin{cases} K_1(b,t)=\dfrac{a}{b\lambda}\left[1+2\sum\limits_{k=1}^{n}(-1)^k\exp\left(-k^2\pi^2\dfrac{at}{b^2}\right)\right] \\ K_2(0,t)=\dfrac{a}{b\lambda}\left[1+2\sum\limits_{k=1}^{n}(-1)^{k+1}\exp\left(-k^2\pi^2\dfrac{at}{b^2}\right)\right] \end{cases}. \quad (38)$$

With regard to formulas (36) and (37), the desired solution for $Q_2(p)$ takes the form

$$Q_2(p)=\frac{T_{low}(p)-T_0(p)-Q_1(p)K_1(p)}{K_2(p)}\ . \quad (39)$$

To find the surface temperature, it is necessary to substitute the known value of $q_1(\varepsilon)$ and original $Q_2(p)$ calculated by formula (39) into initial equation (33). Note that, in going from function $T(b, t)$ to desired function $T(0, t) = T_{surf}(t)$ (i. e., surface temperature), function $\theta(x, t)$ changes to $\theta(b - x, t)$, since coordinate $x = b$ is replaced by $x = 0$. With this in mind, we can write Eq. (33) in the complex form,

$$T_{surf}(p) = T_0(p) + Q_1(p)K_2(p) + Q_2(p)K_1(p) \ . \tag{40}$$

The temperature of the exposed surface can be found using formulas (39) and (40),

$$T_{surf}(p) = T_0(p) + Q_1(p)K_2(p) + \frac{K_1(p)}{K_2(p)}\left[T_{low}(p) - T_0(p) - Q_1(p)K_1(p)\right] \ . \tag{41}$$

Expression (41) shows that, if the sample is thin ($b \to 0$), T_{surf} approaches T_{low}. Indeed, as follows from (38), the expression under the summation sign is an infinitesimal; in this case, $K_1 = K_2$. Substitution of this equality into (32) gives a negligibly small temperature gradient in a plane sample.

Real function T_{surf} is found using the inverse Laplace transformation (Ditkin & Prudnikov, 1966),

$$\frac{1}{2\pi i}\int_{x-i\infty}^{x+i\infty} T_{surf}(p)\exp(pt)\,dp = \begin{cases} T_{surf}(t), if\ t > 0 \\ 0, if\ t < 0 \end{cases} \ . \tag{42}$$

Thus, using the integral transformations, we have derived the expression for the sample temperature in the region exposed to a directed flux of a low-temperature plasma as a function of known parameters. The disadvantage of our method is the difficulty of going to (41). However, this problem can be completely eliminated with program packages.

The model proposed was used to calculate the surface temperature of a silicon dioxide substrate exposed to plasma irradiation. The substrate (0.03 × 0.03 m in area and $b = 0.002$ m in thickness) was exposed to a plasma flux generated by a high-voltage gas discharge in a nonuniform electric field (Kazanskiy et al., 2004) with particle energies reaching 6 keV (Kazanskiy & V.A. Kolpakov, 2003). In air, the current was varied in the range 1–140 mA. In the near-surface layer, the plasma flux incident on the substrate surface produces heat flux q_1, which, having passed through the substrate, turns into flux q_2 (Fig. 12). The lower surface temperature was measured by a precision chromel–copel thermocouple.

The lower surface temperature was found not to exceed 700 K (its variation is presented in Fig. 13). The temperature curve was interpolated by a polynomial the order of which was determined by a given accuracy. In this temperature range, the mean values of the thermophysical parameters of the substrate were taken to be $a = 10^{-5}$ m²/s and $\lambda = 10$ W/(m K) (Kikoin, 1976).

The cathode–anode distance in the gas discharge unit was close to the size of the Aston dark space. In this case, $q_1(\varepsilon)$ was calculated by the techniques described in (V.A. Kolpakov, 2002) as the product of the electron flux by the electron energy (the latter being specified by the accelerating voltage). Such an assumption is valid, since the ion component of the plasma has a low energy compared to the electron one. In addition, the ions rapidly lose energy in collisions with atoms of a working gas. On the other hand, at pressures of 0.1–1.0 Torr and

cathode–substrate distance d = 0.05 m, the number of elastic collisions of electrons with gas atoms is small and the energy loss is insignificant.

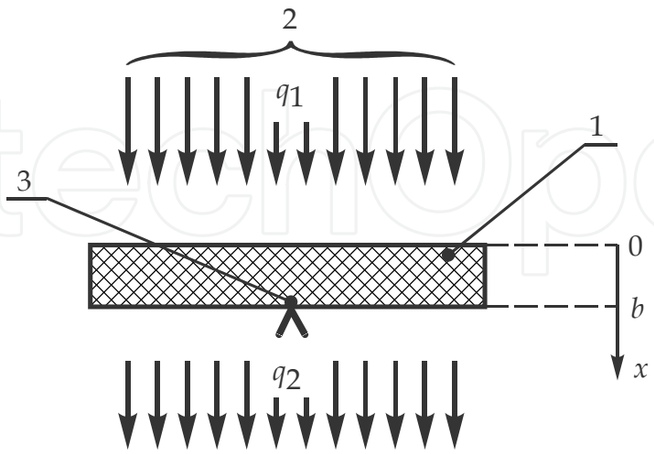

Fig. 12. Irradiation of the sample by the gas-discharge plasma flux: (1) insulating substrate, (2) directed flux of the low-temperature plasma, and (3) temperature sensor at the lower surface

It is known that whether series (34) converges or not depends on the value of at/b^2: the greater this parameter, the better the convergence. To find an exact solution at small at/b^2 (for example, at the initial stage of the process), it is necessary to leave 11–12 terms of the series (Malkovich, 2002). In this study, we took into account 12 terms of sum (34).

As was noted earlier, the boundary-value problem is rather difficult to solve analytically, because (41) contains the ratio of series K_1 and K_2 . Therefore, the proposed algorithm was implemented by applying the Maple 8 program package. Using (41), we constructed the dependences of temperature gradient ΔT in the substrate on the process time (Fig. 14).

As is seen from Fig. 14a, the curves first sharply ascend. This is because the substrate, being thin, heats up rapidly. In other words, incident flux $q_1(\varepsilon)$ passes through the sample almost instantly without noticeable energy losses and goes away from the lower surface, rapidly causing a temperature difference. When the irradiation time is long, the sample heats up at a constant temperature gradient (Fig. 14a).

It is this circumstance that may be responsible for the so-called “thermal shock” (Kartashov, 2001), when thin samples are almost instantly destroyed once the discharge power exceeds a critical value. Indeed, arising thermal stresses are determined by the temperature gradient, which rapidly runs through intermediate values and reaches a maximum virtually at the very beginning of the process (Fig. 14a). The simulation data suggest that the transient time increases as the thermal diffusivity of the sample decreases or it gets thicker, thermal action $q_1(\varepsilon)$ being the same. It is evident that this statement completely agrees with the theory of heat transfer: a more massive sample reaches the stationary state for a longer time. In addition, a material with a lower thermal conductivity will have a higher temperature gradient, which will be established for a longer time. The rigorous solution of this problem implies a combined consideration of the equations of heat transfer and thermoelasticity (Samarskii & Vabishchevich, 1996).

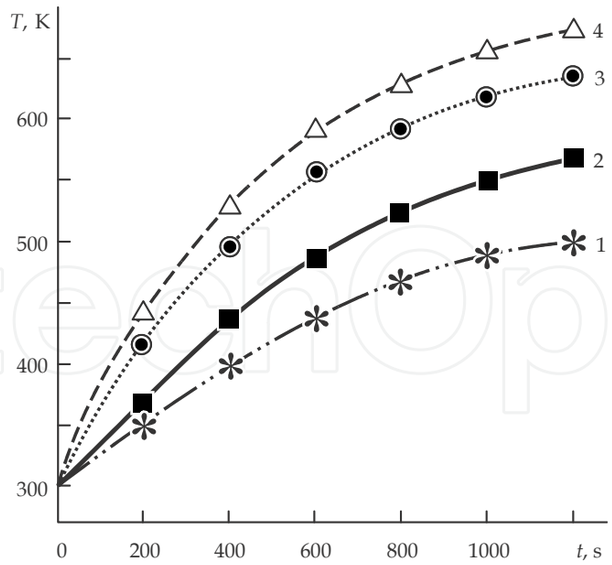

Fig. 13. Lower surface temperature vs. time: I = (1) 50, (2) 80, (3) 120, and (4) 140 mA. The voltage applied to the electrodes is 2 kV, the pressure is 1.5 Torr, and the working gas is air

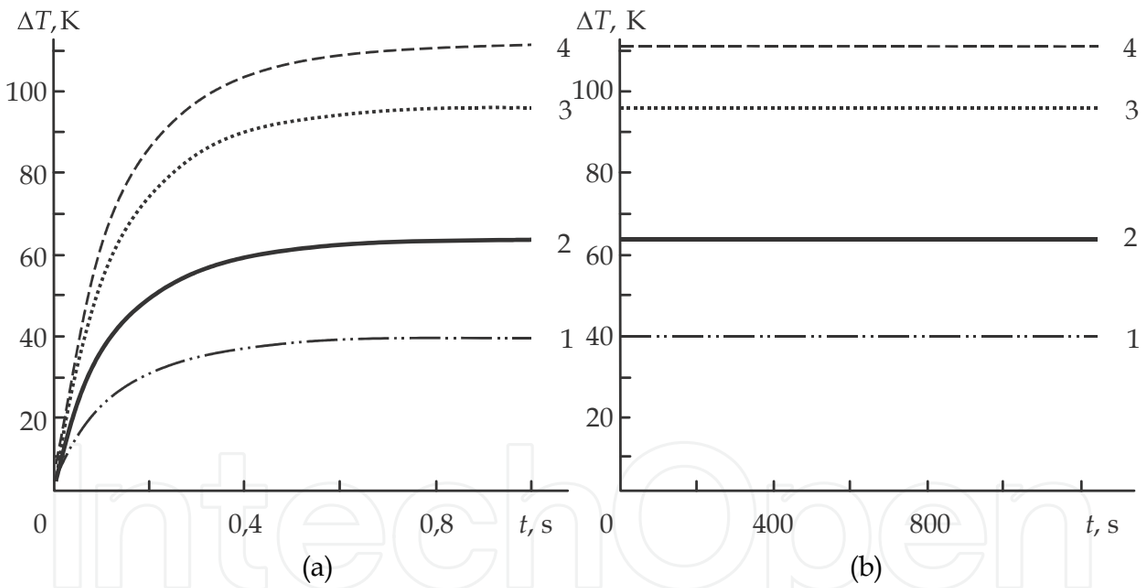

Fig. 14. Temperature difference between the upper and lower surfaces for an irradiation time of (a) 1 and (b) 1200 s. I = (1) 50, (2) 80, (3) 120, and (4) 140 mA

At high t, the temperature difference takes on a constant value (Fig. 14b). Therefore, failure of the sample at the final stage is unlikely. The model proposed was also experimentally verified using KÉF-32 silicon samples measuring 1×1×0.1 cm. The temperature of the sample was controlled by varying the plasma flux irradiation parameters: voltage from 2.6 to 5.2 kV and current from 24 to 80 mA. The irradiation duration was 10 min. The thermophysical parameters of the material were matched to the process conditions. The temperatures of the upper (exposed) and lower surface were measured by a Promin' micropyrometer. The surface temperatures and temperature gradient are listed in the table.

The disagreement between the calculated and experimental values of the temperature difference does not exceed 12%, which confirms the adequacy of the estimation method.
The proposed method was applied for temperature measurement of a surface exposed to an off-electrode plasma flux during research of etch-rate-temperature characteristic. In the plasma etching mode of treatment the etch-rate–temperature characteristic is as shown in Fig. 15a. Notice that for every discharge current the etch rate is maximal at 360 K, the vaporization temperature of SiF_4. This point corresponds to the best conditions for etch-product removal. As the wafer temperature is raised further, the etch rate falls due to decrease in the amount of process gas adsorbed by SiO_2, in accord with earlier results (Ivanovskii, 1986; Kireyev & Danilin, 1983; Kireev et al., 1986).
In the reactive ion etching mode the temperature dependence is not so simple, as can be seen from Fig. 15b. At a discharge current as weak as 50 mA (Fig. 15b, curve 1), the etch rate is almost unaffected by wafer-temperature variation, because the etch rate in this case is determined by the density of F^- ions, as noted above. At 325–360 K, etching is possible because the SiO_2 surface is almost free from particles that could impede etch-product removal.
At stronger discharge currents, quite distinct behavior is observed (Fig. 15b, curves 2–4). The reason is that the removal of SiF_4 is impeded by the species (F^- ions, reactive species, and reaction products) that have accumulated on and underneath the SiO_2 surface, with the result that etching occurs only at wafer temperatures above 360 K, the vaporization temperature of SiF_4. As the wafer temperature increases from 360 K, the etch rate rises to a maximum. Notice that the temperature of maximum etch rate depends on the discharge current, being 390, 422, and 440 K for 80, 120, and 140 mA, respectively. An increase in wafer temperature weakens interatomic bonding in the SiO_2, making the material more susceptible to sputtering. Further, the higher the discharge current, the more ions penetrate the SiO_2 to enter into reactions there. As a result, the product species should migrate more slowly toward the surface with increasing discharge current at a fixed wafer temperature. Higher temperatures are therefore required to remove the products. The sharp fall in etch rate is attributable to increase in ion penetration depth; this factor seriously hinders removal of etch products (SiF_4) with growing wafer temperature. Plasma processing in this case is basically fluorine-ion doping of a SiO_2 surface layer and sputter etching. High temperature breakdown of the photoresist was found to occur at 440 K, showing up as a faster fall in etch rate with wafer temperature (etch rate should be the same in unmasked and opened areas). Breakdown starts from the edges of the mask and causes etch taper (Fig. 16a), which will guide ions just into trenches and so determine the trench profile (Fig. 16b). As the etch taper grows, so do its angles and the etch profile becomes a sinusoid (V.A. Kolpakov, 2002). This property is useful for making diffractive optical elements with a sinusoidal micropattern (Soifer, 2002).

6. Results and discussion: Quality of surface treatment

Figure 17 displays trench profiles obtained by off-electrode plasma etching at discharge currents of 50, 80, and 120 mA and oxygen percentages corresponding to maximum etch rates. Prior to photoresist stripping, processed wafers were examined and found to be free from etch undercut, an indicator of etching anisotropy. It can be seen from Fig. 17 that the profile approaches a vertical-walled pattern with growing discharge current, as predicted earlier. For example, a plasma with a current of 50 mA and a pressure of about 11 Pa is

deficient in F^- ions, but these rarely collide with process-gas molecules and so have energies as high as 100–500 eV (see Eq. (11)). Favorable conditions thus arise for the reflection of F^- ions from trench sidewalls toward the center of the bottom. In this case the sidewalls may deviate from the normal by an angle as large as 70°–75° (Fig. 17a). At a higher density of F^- ions (current 80 mA, pressure 20 Pa), the ions strike the SiO_2 surface with a lower energy and so are more likely to enter surface reactions, mostly at the site of landing. Further, when isolated from other factors, the increase in reactive-species density is known to reduce the sidewall deviation to 10°–20° (Moreau, 1988b).

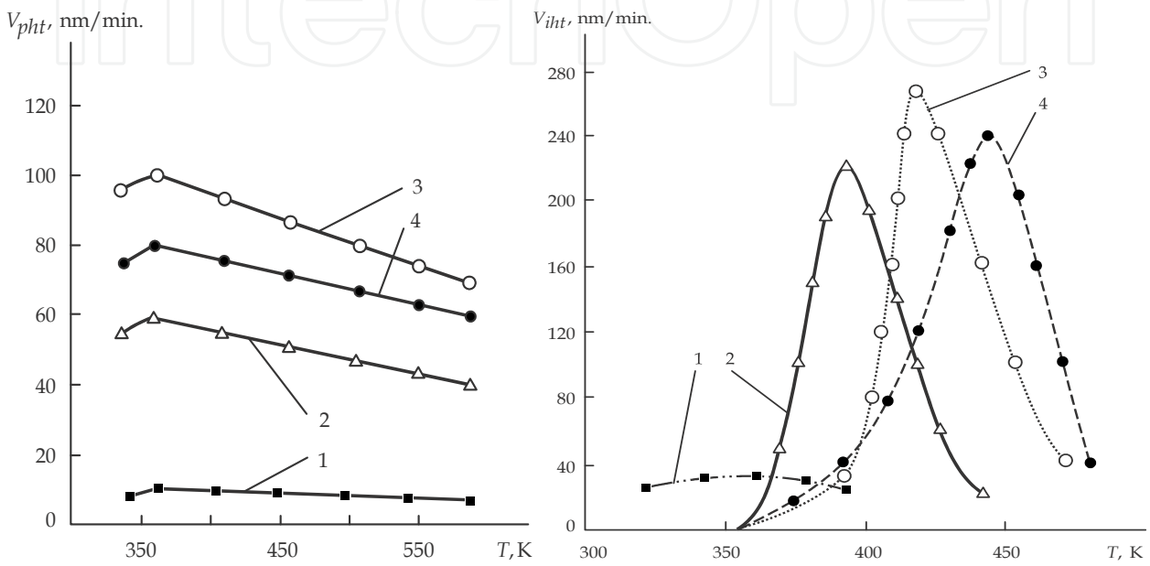

Fig. 15. Etch rate vs. wafer temperature for (a) plasma etching or (b) reactive ion etching in a CF_4–O_2 plasma at discharge currents of (1) 50, (2) 80, (3) 120, and (4) 140 mA

Figure 17b,c shows that the trench bottoms meet the requirements of microelectronics manufacturing: they are smooth and free from acute angles. Moreover, etching at 120–140 mA and 25–33 Pa was found to produce trenches with vertical walls and a smooth bottom (Fig. 17d, e, f). Finally, the pressures employed satisfy the conditions given in (Orlikovskiy, 1999a). Thus, all the trench profiles presented could find use in microelectronics (Moreau, 1988b; Muller & Kamins, 1986) and diffractive optics (Soifer, 2002).

Off-electrode plasma etching in a CF_4–O_2 plasma was also applied to other materials used in microelectronics, as well as in diffractive optics. The respective etch rates are listed in the table. At the same time, it was observed that fairly thick deposit is formed on the cathode during etching (Fig. 18). Figure 19 is an x-ray diffraction pattern (Mirkin, 1961) from the deposit; it indicates elements and compounds present in the process gas (*C*), the etched material (SiO_2, *SiC*, *Si*, As_2S_3, and *C*), and the etch mask (Cr_2O_3, CrO_3, *C*, and H_2). Cathode deposit also includes large amounts of compounds containing the cathode material and different oxides. On the other hand, it is free from fluorine, a fact suggesting that fluorine is totally involved in etching (as part of reactive species). Moreover, the presence of the etched material in the deposit implies that the plasma ensures etch-product removal. It follows that the working plasma species (F^- ions) move toward the wafer, whereas the product ones

toward the cathode. This result supports the mechanisms presented above. It is in accord with earlier research (V.A. Kolpakov, 2002).

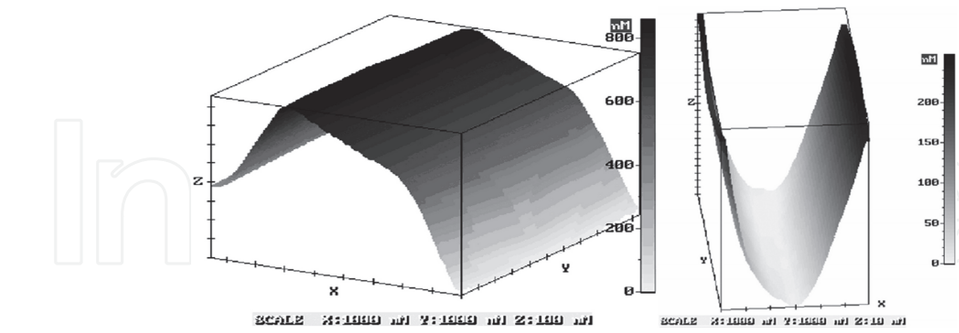

(a) (b)

Fig. 16. (a) Etch taper due to high-temperature photoresist breakdown and (b) the corresponding trench profile. Etching is carried out at a discharge current of 140 mA, a cathode voltage of 2 kV, and a wafer temperature of 440 K

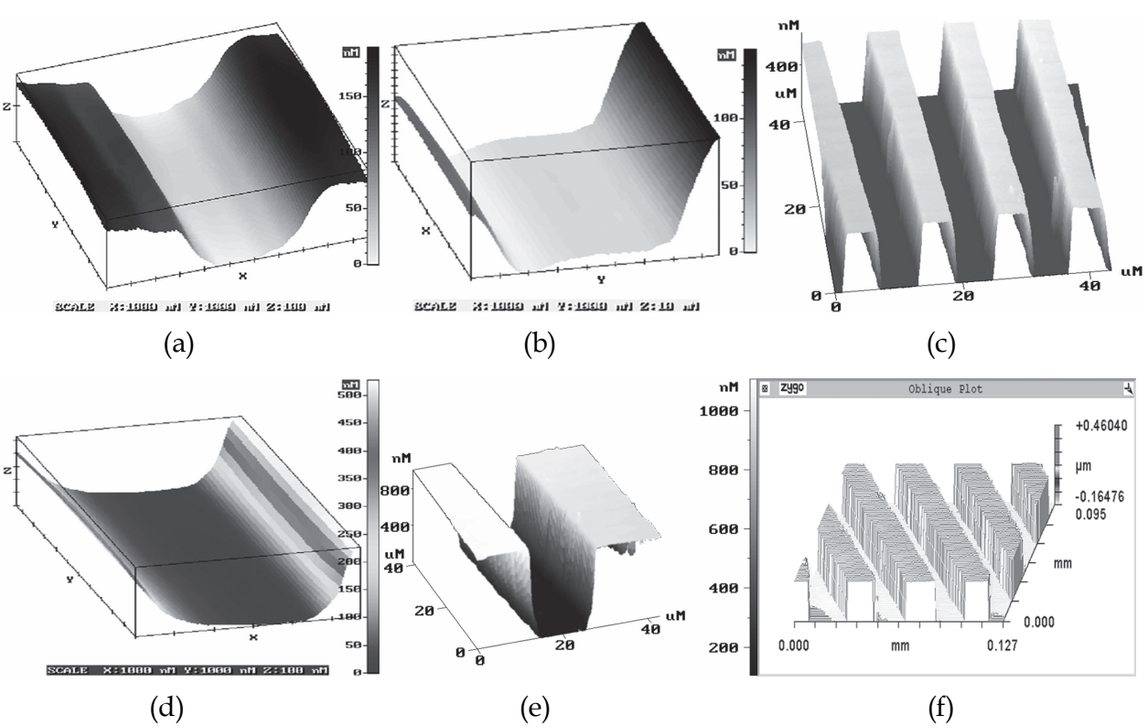

(a) (b) (c)

(d) (e) (f)

Fig. 17. Images of trenches obtained by etching in CF_4–O_2 plasma at different discharge currents, optimal oxygen percentages, and a cathode voltage of 2 kV. The discharge currents are (a) 50, (b, c) 80, and (d, e, f) 120 mA. The oxygen percentages are (a) 0.5, (b, c) 0.8, and (d, e, f) 1.3%

Thus, even with highly contaminated process gas and wafer surface, off-electrode plasma etching does not involve interactions other than a useful one (between reactive species and wafer-surface molecules), allowing one to take less expensive gases.

Etching uniformity is among major concerns in microfabrication, because etch rate can vary in a complicated manner over the wafer surface (Ivanovskii, 1986; Kovalevsky et al., 2002; Poulsen & Brochu, 1973). In essence, all the recent improvements in plasma etching technology aim to give high etching uniformity and rate; hence the high complexity and cost of the equipment.

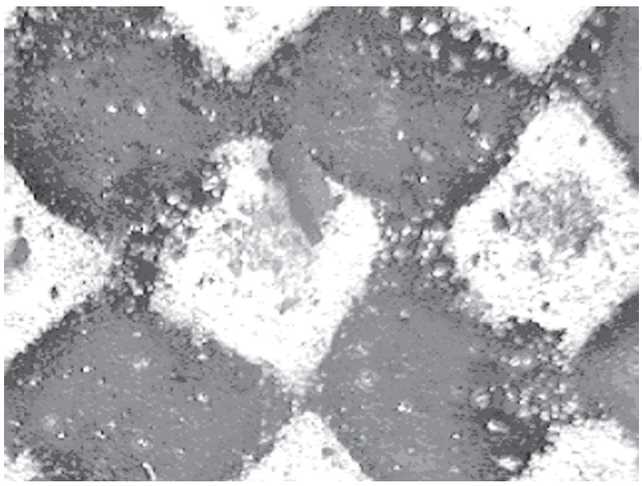

Fig. 18. Cathode surface after etching (magnification ×36)

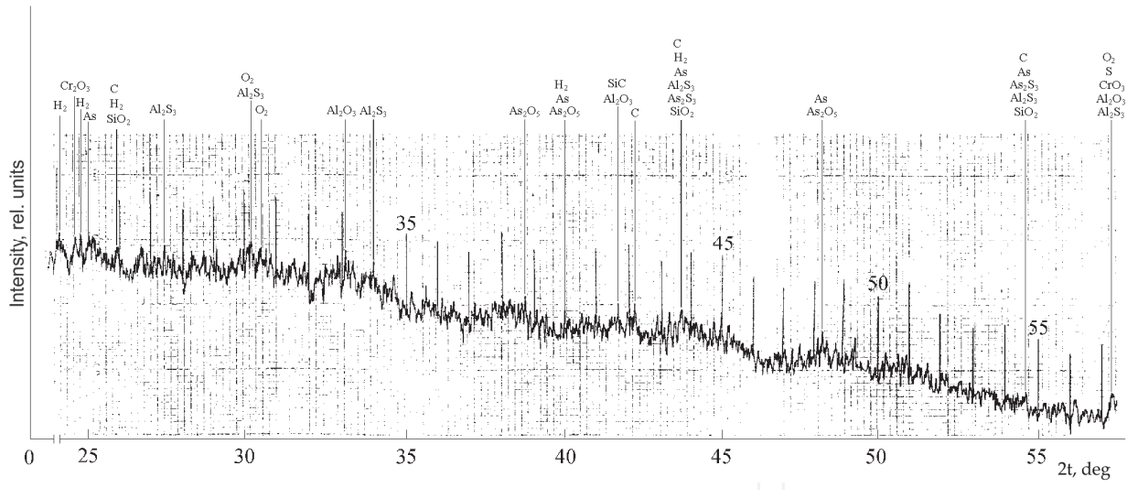

Fig. 19. X-ray diffraction pattern (wavelength 0.154 nm) from cathode deposit, with t denoting the x-ray reflection angle from the atomic planes

Our evaluation of off-electrode plasma etching in terms of uniformity, for a wafer of diameter 100 mm, showed that both the plasma etching and the reactive ion etching mode are uniform within 1% over the whole wafer. Etch profile was measured in different areas on the wafer, and etch depth was found to be almost the same. The minor variations in etch depth are in all likelihood linked with surface imperfections (lattice defects, contamination, etc.) rather than the plasma conditions.

7. Conclusion

It has been shown that a major feature that distinguishes the high-voltage gas discharge from the existing discharges is that the former can be induced in the dark Aston space, provided an anode hole. This feature allows to generate a low-temperature plasma flux outside the electrode gap.

Based on our experiments, a method for estimating the surface temperature of a sample irradiated by a low-temperature plasma flux is produced. The relationships obtained in this paper make it possible to evaluate the surface temperature directly at the site exposed to the plasma flux. A slight excess of the theoretical estimate seems to be associated with the fact that the plasma flux is incompletely absorbed by the solid: part of the flux is reflected from the surface, decreasing the gradient. During ion–plasma processing, the temperature gradient in the sample may become very high according to the geometry and material of the sample, as well as to the amount of the thermal action.

The method makes it possible to trace the surface temperature of a sample being etched by directed low-temperature plasma fluxes in a vacuum. This opens the way of improving the quality of micro- and nanostructures by stabilizing the process temperature and optimizing the rate of etching in the low-temperature plasma.

The phenomenon of thermal shock taking place at ion–plasma processing of flat surfaces is theoretically explained. It is shown that the failure probability of thin samples is the highest early in irradiation under the action of rapidly increasing thermal stresses. To determine the critical power of the discharge, it is necessary to jointly solve the equations of heat conduction and thermoelasticity.

Among disadvantages of the method is the neglect of the temperature dependence of thermophysical parameters. This point becomes critical for semiconductors operating in a wide temperature range. As a result, the temperature gradient versus process time dependence becomes ambiguous. A more rigorous solution can be obtained by applying numerical methods to the direct problem of heat conduction with mixed boundary conditions. This would be a logical extension of this investigation.

8. Acknowledgment

The work was financially supported by the RF Presidential grant # NSH-7414.2010.9, the Program of the President of the Russian Federation for Supporting Young Russian Scientists (grant no. MD-1041.2011.2) and the Carl Zeiss grant # SPBGU 7/11 KTS.

9. References

Orlikovskiy, A.A. (1999a). Plasma Processes in Micro- and Nanoelectronics, Part 1: Reactive Ion Etching. *Mikroelektronika*, Vol. 28, No. 5, pp. 344–362 (In Russian)

Alifanov, O. M. (1983). *Inzhen.Fizich. Zhurnal*. Vol. 45, No. 5, p.p. 742-752 (In Russian)

Alifanov, O. M. (1994). *Inverse Heat Transfer Problem*, Springer, New York

Bartenev, G. M. & Barteneva, A. G. (1992). *Relaxation Properties of Polymers*, Khimiya, Moscow (In Russian)

Bechstedt, F. & Enderlein, R. (1988). *Semiconductor Surfaces and Interfaces*, Akademie-Verlag, Berlin

Carslaw, H. S. & Jaeger, J. C. (1956). *Conduction of Heat in Solids*, Clarendon Press, Oxford

Chernetsky, A. V. (1969). *Introduction into Plasma Physics*, Atomizdat Publishers, Moscow (In Russian)

Chernyaev, V.N. (1987). *Fiziko-khimicheskie protsessy v tekhnologii REA (Physical and Chemical Processes in Electronics Manufacture)*, Vysshaya Shkola, Moscow (In Russian)

Ditkin, V. A. & Prudnikov, A. P. (1966). *Integral Transforms and Operational Calculus*, Pergamon, Oxford

Doh Hyun-Ho et al. (1997). Effects of bias frequency on reactive ion etching lag in an electron cyclotron resonance plasma etching system. *J.Vac. Sci. and Technol. A., Pt 1,* Vol.15, No. 3, p.p. 664-667

Flamm, D.L. (1979). Measurements and Mechanisms of Etchant Production During the Plasma Oxidation of CF_4 and C_2F_6. *Solid State Technol.*, Vol. 22, No. 4, pp. 109–116

Gerlach-Meyer, V. (1981). Ion Enhanced Gas-Surface Reactions: A Kinetic Model for the Etching Mechanism. *Surface Sci.*, Vol. 103, No. 213, pp. 524–534

Harsberger, W.R. & Porter, R.A. (1979). Spectroscopic Analysis of RF Plasmas. *Solid State Technol.,* Vol. 22, No. 4, pp. 90–103

Hebner, G.A. et al. (1999). Influence of surface material on the boron chloride density in inductively coupled discharges. *J.Vac. Sci. and Technol. A.,* Vol.17, No. 6, p.p. 3218-3224

Horiike, Y. (1983). Dry Etching: An Overview. *Jap. Annual Revue in Electronics, Computers and Telecommunicated Semiconductor Technologies*, Vol. 8, pp. 55–72

Ivanovskii, G.F. (1986). *Ionno-plazmennaya obrabotka materialov (Plasma and Ion Surface Engineering)*, Radio i Svyaz', Moscow (In Russian)

Izmailov, S. V. (1939). On the thermal theory of electron emission under the impact of fast ions. *Russian Journal of Experimental and Theoretical Physics*, Vol.9, No. 12, p.p. 1473 – 1483 (In Russian)

Kartashov, E. M. (2001). *Analytical Methods in the Theory of Heat Conduction in Solids*, Vysshaya Shkola, Moscow (In Russian)

Kazanskiy, N.L. & Kolpakov, V.A. (2003). Studies into mechanisms of generating a low-temperature plasma in high-voltage gas discharge. *Computer Optics*, No. 25, p.p. 112-117 (In Russian)

Kazanskiy, N. L. et al. (2004). Anisotropic Etching of SiO_2 in High-Voltage Gas-Discharge Plasmas. *Russian Microelectronics*, Vol. 33, No. 3, p.p. 169-182

Kikoin, I. K. (Ed.). (1976). *Tables of Physical Quantities*, Atomizdat, Moscow (In Russian)

Kireyev, V. Yu. & Danilin, B. S. (1983). *Plasmo-chemical and ion-chemical etching of microstructures*, Radio i Svyaz (Radio and Communications) Publishers, Moscow (In Russian)

Kireev, V.Yu. et al., (1986). Ion-Enhanced Dry Etching. *Elektron. Obrab. Mater. (Electron Treatment of Materials),* No. 67, pp. 40–43 (In Russian)

Kolpakov, A.I. & Kolpakov, V.A. (1999). Dragging of Silicon Atoms by Vacancies Created in Molten Aluminum under Ion–Electron Irradiation. *Technical Physics Letters*, Vol. 25, No. 15, p. 618

Kolpakov, V.A. (2002). Modeling the High-Voltage Gas-Discharge Plasma Etching of SiO_2. *Mikroelektronika,* Vol. 31, No. 6, pp. 431–440 (In Russian)

Kolpakov, A. I. et al. (1996). Ion-plasma cleaning of low-power relay contacts. *Electronics Industry*, No. 5, p.p. 41-44 (In Russian)

Kolpakov, A. I. & Rastegayev, V. P. (1979). *Calculating the electric field of a high-voltage gas discharge gun*, VINITI, Moscow (In Russian)

Kolpakov, V. A. (2004). *Candidate's Dissertation*, SGAU & ISOI RAN, Samara (In Russian)

Kolpakov, V. A. (2006). Studying an Adhesion Mechanism in Metal – Dielectric Structures Following the Surface Ion-Electron Bombardment. Part 1. Modeling an Adhesion Enhancement Mechanism. *Phys. and Chem. of Mat. Proc.*, No. 5, pp. 41-48 (In Russian)

Komine Kenji et al. (1996). Residuals caused by the CF_4 gas plasma etching process. *Jap. J. Appl. Phys. Pt.1*, Vol. 35, No. 5b, p.p. 3010-3014

Komov, A.N. et al. (1984). Electron-Beam Soldering Machine for Semiconductor Devices. *Prib. Tekh. Eksp. (Scientific Instruments and Methods)*, No. 5, pp. 218–220 (In Russian)

Kovalevsky, A. A. et al. (2002). Studies into the process of isotropic plasmo-chemical etching of silicon dioxide films. *Mikroelektronika*, Vol. 31, No. 5, p.p. 344-349 (In Russian)

Malkovich, R. Sh. (2002). *Technical Physics Letters*, Vol. 28, No. 21, p. 923

Matare, G. (1974). *Electronics of semiconductor defects*, Mir Publishers, Moscow (In Russian)

McLane, G.F. et al. (1997). Dry etching of germanium in magnetron enhanced SF_6 plasmas. *J.Vac. Sci. and Technol. B.*, Vol. 15, No. 4, p.p. 990-992

Mirkin, L.I. (1961). *Spravochnik po rentgenostrukturnomu analizu polikristallov (Handbook of X-ray Crystallography for Polycrystalline Materials)*, Gosudarstvennoe Izdatel'stvo Fiziko-Matematicheskoi Literatury Publisher, Moscow (In Russian)

Miyata Koji et al. (1996). CF_x radical generation by plasma interaction with fluorocarbon films on the reactor wall. *J.Vac. Sci. and Technol. A.*, Vol. 14, No. 4, p.p. 2083-2087

Molokovsky, S. I. & Sushkov, A. D. (1991). *High-intensity Electron and Ion Beams*, Energoatomizdat Publishers, Moscow (In Russian)

Moreau, W. M. (1988a). *Semiconductor Lithography: Principles, Practices and Materials. Chap. 1,* Plenum, New York

Moreau, W.M. (1988b). *Semiconductor Lithography: Principles, Practices, and Materials. Chap. 2*, Plenum, New York

Muller, R.S. & Kamins, T.I. (1986). *Device Electronics for Integrated Circuits*, Wiley, New York

Orlikovskiy, A.A. (1999b). Plasma Processes in Micro- and Nanoelectronics, Part 2: New-Generation Plasmochemical Reactors in Microelectronics. *Mikroelektronika*, Vol. 28, No. 6, pp. 415–426 (In Russian)

Popov, V. K. (1967). *Fiz. Khim. Obrab. Mater. (Physics and Chemistry of Materials Processing)*, No. 4, p.p. 11-24 (In Russian)

Poulsen, R.G. & Brochu, M. (1973). *Importance of Temperature and Temperature Control in Plasma Etching*, Si Bricond Silicon, New-Jersey

Raizer, Yu.P. (1987). *Fizika gazovogo razryada (Gas-Discharge Physics)*, Nauka, Moscow (In Russian)

Rykalin, N. N. et al. (1978). *Principles of Electron-beam Material Processing*, Mashinostroyenie (Mechanical Engineering) Publishers, Moscow (In Russian)

Samarskii, A. A. & Vabishchevich, P. N. (1996). *Computational Heat Transfer*, Wiley, Chichester

Sarychev, M. E. (1992). Non-liner Diffusion Model of Polymer Resist Plasma-chemical Etching Process. Simulation of Technological Processes of Microelectronics. *Tr. FTIAN (FTIAN Annals)*, Vol. 3, p.p. 74-84 (In Russian)

Soifer, V.A. (Ed.). (2002). *Methods for Computer Design of Diffractive Optical Elements*, Wiley, New York

Tikhonov, A. N. & Samarskii, A. A. (1964). *Equations of Mathematical Physics*, Pergamon, Oxford

Tikhonov, A. N. & Arsenin, V. Ya. (1977). *Solutions of Ill-Posed Problems*, Halsted, New York

Vabishchevich, P. N. & Pulatov, P. A. (1986). *Inzhen.Fizich. Zhurnal.* Vol. 51, No. 3, p.p. 470-474 (In Russian)

Vagner, I.V. et al. (1974). Simple Beam-Forming Arrangement for Generating Arbitrarily Shaped Electron Beams under High-Voltage Gas Discharge. *Zh. Tekh. Fiz.(Russian Journal of Technical Physics)*, Vol. 44, No. 8, pp. 1669–1674 (In Russian)

Valiev, K. A. et al. (1985). Polymer Plasma-chemical Etching Mechanism. *Dokl. Akad. Nauk SSSR (Sov. Phys. Dokl)*, Vol. 30, p. 609 (In Russian)

Valiev, K. A. et al. (1987). Investigation of Etching Kinetics of Polymetilmetacrelat in Low-temperature Plasma. *Poverkhnost' (Surface)*, No. 1, p.p. 53-57 (In Russian)

Woodworth, J.R. et al. (1997). Effect of bumps on the wafer on ion distribution functions in high-density argon and argon-chlorine discharges. *Appl. Phys. Lett.*, Vol. 70, No. 15, p.p. 1947-1949

Heat Transfer - Engineering Applications

Edited by Prof. Vyacheslav Vikhrenko

ISBN 978-953-307-361-3
Hard cover, 400 pages
Publisher InTech
Published online 22, December, 2011
Published in print edition December, 2011

Heat transfer is involved in numerous industrial technologies. This interdisciplinary book comprises 16 chapters dealing with combined action of heat transfer and concomitant processes. Five chapters of its first section discuss heat effects due to laser, ion and plasma-solid interaction. In eight chapters of the second section engineering applications of heat conduction equations to the curing reaction kinetics in manufacturing process, their combination with mass transport or ohmic and dielectric losses, heat conduction in metallic porous media and power cables are considered. Analysis of the safety of mine hoist under influence of heat produced by mechanical friction, heat transfer in boilers and internal combustion engine chambers, management for ultrahigh strength steel manufacturing are described in this section as well. Three chapters of the last third section are devoted to air cooling of electronic devices.

InTech Europe
University Campus STeP Ri
Slavka Krautzeka 83/A
51000 Rijeka, Croatia
Phone: +385 (51) 770 447
Fax: +385 (51) 686 166
www.intechopen.com

InTech China
Unit 405, Office Block, Hotel Equatorial Shanghai
No.65, Yan An Road (West), Shanghai, 200040, China
中国上海市延安西路65号上海国际贵都大饭店办公楼405单元
Phone: +86-21-62489820
Fax: +86-21-62489821

IntechOpen